Federated Learning of Quantile Inference under Local Differential Privacy

Leheng Cai[†]
Department of Statistics and Data Science
Tsinghua University
Beijing 100084, China
`cailh22@mails.tsinghua.edu.cn`

Qirui Hu[†*]
School of Statistics and Data Science,
Shanghai University of Finance and Economics
Institute of Big Data Research,
Shanghai University of Finance and Economics
Shanghai 200443, China
`huqirui@mail.shufe.edu.cn`

Shuyuan Wu[†]
School of Statistics and Data Science,
Shanghai University of Finance and Economics
Shanghai 200433, China
`wushuyuan@mail.sufe.edu.cn`

Abstract

In this paper, we investigate federated learning for quantile inference under local differential privacy (LDP). We propose an estimator based on local stochastic gradient descent (SGD), whose local gradients are perturbed via a randomized mechanism with global parameters, making the procedure tolerant of communication and storage constraints without compromising statistical efficiency. Although the quantile loss and its corresponding gradient do not satisfy standard smoothness conditions typically assumed in existing literature, we establish asymptotic normality for our estimator as well as a functional central limit theorem. The proposed method accommodates data heterogeneity and allows each server to operate with an individual privacy budget. Furthermore, we construct confidence intervals for the target value through a self-normalization approach, thereby circumventing the need to estimate additional nuisance parameters. Extensive numerical experiments and real data application validate the theoretical guarantees of the proposed methodology.

1 Introduction

Modern data ecosystems increasingly require distributional guarantees rather than simple averages. For instance, a national hospital network may track the 0.9 quantile of emergency waiting times across sites to ensure that "nine out of ten patients are seen within T minutes" (Yadlowsky et al., 2025), while financial institutions assess tail risk via value-at-risk or expected shortfall under strict confidentiality constraints (Barbaglia et al., 2023; Chen, 2008; Wang et al., 2012). In both settings, the target is a quantile of a heterogeneous, possibly heavy-tailed distribution, and the scientific goals—comparing tail performance, checking compliance, or detecting post-intervention shifts—require full inferential tools, not just point estimates.

Quantile methods naturally support these tasks, revealing heterogeneity and tail behavior often invisible to means (Angrist et al., 2006; Kallus et al., 2024; Chernozhukov & Fernández-Val, 2011; Chernozhukov & Hansen, 2005; He et al., 2023; Hu et al., 2022; Chen et al., 2023). Yet the data required for such inference are increasingly distributed: hospitals, banks, and user-facing services each hold their own records, and centralizing raw data is often infeasible due to communication, storage, privacy, and regulatory barriers.

---

[*]Corresponding author
[†]The authors are listed in alphabetical order with equal contribution

These challenges motivate federated learning (McMahan et al., 2017; Konečný et al., 2016; Liu et al., 2020; Tian et al., 2023), where a server coordinates updates from many clients without collecting their raw data. Local SGD can be optimal under i.i.d. data (Stich, 2018; Li et al., 2020; Chen et al., 2022), but realistic federated environments are heterogeneous in distributions, sample sizes, and even target quantiles, complicating optimization and inference and prompting methods based on regularization, momentum, and worst-case analysis (Hu et al., 2024; Li et al., 2020; 2025; 2022).

At the same time, protections limited to servers or silos are no longer considered sufficient. Breaches of medical and financial records show that server-side DP alone (Dwork et al., 2006) cannot prevent disclosure when the custodian is compromised. Local differential privacy (LDP) mitigates this risk by randomizing each individual record before transmission (Duchi et al., 2013); deployed systems such as Google's RAPPOR, Apple's telemetry, and Windows diagnostics demonstrate its practicality (Erlingsson et al., 2014; Ding et al., 2017).

Differentially private federated learning merges these ideas and has gained substantial interest (Agarwal et al., 2018; Shi et al., 2022; Ma et al., 2022; Liu et al., 2023a). As emphasized by Lowy & Razaviyayn (2023), privacy guarantees vary by trust assumptions; LDP corresponds to the most conservative regime in which individuals trust neither server nor silo. Recent work studies LDP in distributed settings for generalized linear models, mean estimation, and related tasks (Zhao et al., 2020; Shen et al., 2023; Jiang et al., 2022), but primarily from an estimation perspective. For quantiles, existing LDP methods are either single-machine procedures that ignore client heterogeneity (Huang et al., 2021; Liu et al., 2023b) or provide point estimators without general inferential guarantees.

In contrast, our focus is on quantile inference under LDP in a federated, heterogeneous environment. Concretely, we consider a setting in which many clients, each holding local data drawn from potentially different distributions and targeting possibly different quantile levels, collaborate to estimate and infer a global quantile while ensuring that every message they send is locally private.

We illustrate with a simple example. Consider collaboratively estimating the national median annual income using state-level data from the United States, where each state is treated as a client. First, income distributions typically vary across states (see Figure 1(i)). Second, privacy preferences can differ across states due to cultural norms and development levels (Milberg et al., 2000; Bellman et al., 2004). Figure 1(ii) shows how the released information can vary under different privacy budgets. Due to such heterogeneity, a direct application of the divide-and-conquer method, which combines local LDP estimators from Liu et al. (2023b) designed for a single client, can yield estimation with significant bias and invalid inference.
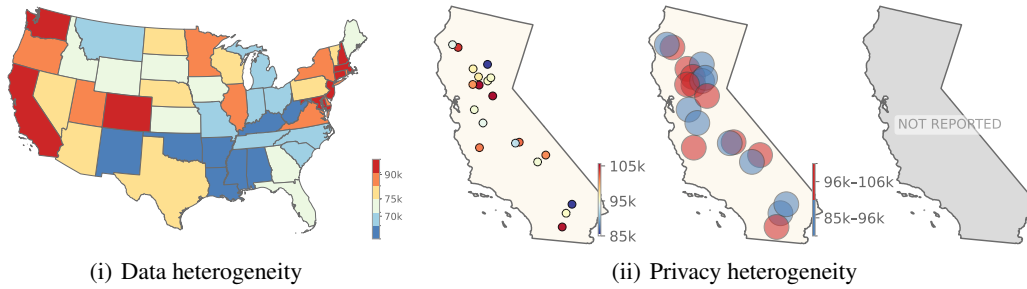

| (i) Data heterogeneity | (ii) Privacy heterogeneity |

Figure 1: Illustration of client heterogeneity. Income data source: U.S. Census Bureau (`https://data.census.gov/table/ACSST5Y2023.S1901?g=010XX00US0400000`). Panel (i) shows median annual income by state. Panel (ii) shows three income disclosure schemes under different privacy budgets: (a) each individual release true income; (b) each individual release an income interval; and (c) withholding release.

> The key question is: Can we design a federated procedure for quantile estimation under LDP that admits valid confidence intervals and hypothesis tests, while accommodating client heterogeneity and non-smooth loss functions?

Answering this question is challenging for at least three reasons. First, inference requires not only a limiting distribution for the estimator, but also a consistent estimator of its asymptotic variance. For SGD-based procedures, such variance estimators typically involve the Hessian of a smooth loss (Chen et al., 2020); yet quantile losses are non-smooth and heterogeneous across clients. Second, in the LDP regime, only privatized gradients are observed, so naive variance estimation may consume additional privacy budget or demand data-splitting. Third, federated quantile algorithms must remain robust to heterogeneous loss functions and client-level privacy parameters, which further complicates both optimization and asymptotic analysis.

In this paper, our contributions can be summarized as follows:

1. We propose a novel federated learning algorithm for quantile inference under LDP. Our method accommodates client-level heterogeneity in quantile targets, privacy budgets, and data distributions, thereby enhancing the applicability of quantile inference in realistic federated environments.

2. We first design an LDP mechanism that effectively reduces the federated quantile estimation problem to an equivalent non-private setting. Exploiting this reduction, we establish the estimator's asymptotic normality and derive a functional central limit theorem without average-smoothness condition on the loss function. To the best of our knowledge, this constitutes the first weak-convergence result for local SGD when the loss does not satisfy the usual average-smoothness condition (Li et al., 2022; Xie et al., 2024; Zhu et al., 2024).

3. Building on these non-private asymptotic results, we develop an LDP inference procedure for federated quantile estimation. By employing a self-normalization technique, we avoid direct estimation of the asymptotic variance, instead constructing confidence intervals that automatically eliminate the unknown variance term. These procedures can be also conducted in non-DP case.

The remainder of the paper is organized as follows. Section 2 introduces the formal problem setup, background, and notation, and presents our LDP mechanism and federated quantile estimator. Section 3 develops the asymptotic theory, including weak convergence and self-normalized inference. Section 4 reports numerical experiments and a real-data application illustrating the practical performance and robustness of our method. Notations can refer to Table S.1 in Appendix A.1. All technical proofs and additional simulation results are deferred to the Appendices B and C.

2 METHODOLOGIES

First, we recall the definitions of central and local differential privacy. We then describe our problem setting and algorithmic details.

Definition 1 (Central Differential Privacy, CDP (Dwork et al., 2006)). *A randomized algorithm $\mathcal{A}$ operating on a dataset S is (ϵ, δ)-differentially private if, for any pair of datasets S and S' differing in a single record and for any measurable set E,*

$$\Pr\big(\mathcal{A}(S) \in E\big) \leq e^\epsilon \Pr\big(\mathcal{A}(S') \in E\big) + \delta.$$

When $\delta = 0$, $\mathcal{A}$ is called ϵ-DP.

Definition 2 (Local Differential Privacy, LDP (Joseph et al., 2019)). *A family of randomized mappings $R : X \to Y$ is (ϵ, δ)-locally differentially private if, for every pair of inputs $x, x' \in X$ and every measurable subset $E \subseteq Y$,*

$$\Pr\big(R(x) \in E\big) \leq e^\epsilon \Pr\big(R(x') \in E\big) + \delta.$$

Under CDP, a trusted curator collects raw data and adds noise before release, simplifying algorithm design and typically incurring only an $\mathcal{O}(1/n)$ loss in accuracy (Cai et al., 2021), so the privatized estimator $\widehat{\theta}_{\mathrm{CDP}}$ often satisfies $\widehat{\theta}_{\mathrm{CDP}} - \widehat{\theta}_{\mathrm{nonDP}} = \mathcal{O}_p(n^{-1})$, shares the same $\sqrt{n}$-scaled asymptotic law as the non-private estimator, and permits recovery of its asymptotic variance at modest additional privacy cost. In contrast, under the non-adaptive LDP model (Cheu et al., 2019, Definitions 2.3 and 2.6), each user i with private value X_i applies a fixed randomized mechanism R_i satisfying (ϵ, δ)-DP and reports only the perturbed output, so inference must rely solely on locally privatized

data; the typical error rate deteriorates to $\widehat{\theta}_{\text{LDP}} - \widehat{\theta}_{\text{nonDP}} = \mathcal{O}_p(n^{-1/2})$, which alters the limiting distribution, inflates the asymptotic variance, and generally makes consistent variance estimation from data collected solely for point estimation infeasible.

We consider a federated learning framework involving K clients, each independently holding a local dataset i.i.d. drawn from an unknown distribution $\mathcal{P}_k$ with cumulative distribution function (CDF) F_k and density function f_k (Li et al., 2022). For p_k weight assigned to client k, global quantile level $\tau \in (0,1)$, the goal is to collaboratively estimate the global quantile $Q^\star$, which satisfies that $\sum_{k=1}^{K} p_k F_k(Q^\star) = \tau$. Our objective $Q^\star$ can be obtained by solving the following optimization problem associated with the global loss, which is defined as a weighted sum of the local losses:

$$Q^\star = \underset{Q \in \Theta}{\arg\min}\, \mathcal{L}(Q) \stackrel{\text{def}}{=} \underset{Q \in \Theta}{\arg\min} \sum_{k=1}^{K} p_k \mathcal{L}_{\tau_k}(Q) \stackrel{\text{def}}{=} \underset{Q \in \Theta}{\arg\min} \sum_{k=1}^{K} p_k \mathbb{E}_{x_k \sim \mathcal{P}_k}\{\ell_{\tau_k}(x_k, Q)\}. \quad (2.1)$$

Here, the function $\ell_{\tau_k}(x, Q)$ represents the check loss function defined as:

$$\ell_{\tau_k}(x, Q) = (x - Q)\{\tau_k - \mathbb{I}(x < Q)\}, \quad (2.2)$$

where $\mathbb{I}(\cdot)$ is the indicator function. Besides, x_k is the sample generated from $\mathcal{P}_k$, and $\tau_k \in (0,1)$ is the local quantile level satisfying $\sum_{k=1}^{K} p_k \tau_k = \tau$. Therefore, our framework also covers federated quantile loss optimization problems in which each local loss corresponds to a level τ_k, and the global objective level τ aggregates these local target levels through $\sum_{k=1}^{K} p_k \tau_k$. Note that we require only the knowledge of τ, rather than each individual τ_k. In the following, we denote $F_k(Q^\star) = Q_k$, and considers the parameter space Θ is bounded; see Gu & Chen (2023).

As noted in the introduction, to improve communication efficiency we consider a local-SGD–based estimator. Let $\mathcal{I} = \{t_0, t_1, \dots, t_T\}$ for $t_0 < t_1 < \cdots < t_T$ denote the ordered set of communication iterations. At each $t \in \mathcal{I}$, the global server receives the local updates and broadcasts the aggregated value to all K clients; otherwise, the updates are performed locally on each client. Specifically, for $k = 1, \dots, K$,

$$q_{t+1}^k = \begin{cases} q_t^k - \eta_t \{\mathbb{I}(x_t^k < q_t^k) - \tau_k\}, & t \notin \mathcal{I}, \\ \sum_{m=1}^{K} p_m [q_t^m - \eta_t \{\mathbb{I}(x_t^m < q_t^m) - \tau_m\}], & t \in \mathcal{I}. \end{cases}$$

Here η_t is the predetermined learning rate, and x_t^k is an observation from the local dataset held by client k at iteration t. The final estimator is of Polyak–Ruppert type, obtained by averaging the aggregated historical iterates:

$$\widetilde{Q}_T = \frac{1}{T} \sum_{m=1}^{T} \sum_{k=1}^{K} p_k q_{t_m}^k.$$

The communication and statistical efficiency are determined by the interval length $E_m := t_m - t_{m-1}$ for $m \in \mathbb{N}^+$. If $E_m = 1$, the local clients must communicate with the global server at every iteration. In this scenario, the approach reduces to parallel SGD, which, as noted by Li et al. (2022), may achieve the Cramér-Rao lower bound and thus serve as an efficient estimator for certain smooth loss functions. Conversely, if communication is performed only once at the final iteration (i.e., $|\mathcal{I}| = 1$), then the estimator degenerates to a divide-and-conquer (DC) estimator. In this case, minimizing the loss function (2.1) becomes a distributed learning problem. However, as pointed out by Gu & Chen (2023), the divide-and-conquer estimator may still be statistically inefficient for certain weight choices. Therefore, a careful balance must be struck between communication and statistical efficiency. For a general positive interval $E_m > 0$, the local SGD method allows us to find an appropriate choice of E_m that can ensure an optimal trade-off between these efficiencies.

On the other hand, the data collected from each client may be subject to privacy protection policies, particularly in surveys involving sensitive information such as income or health status. For the local quantile loss function (2.2), we observe that the structure of its gradient resembles a binary response. This motivates us to incorporate an LDP mechanism based on randomized response and permutation, following the framework of Liu et al. (2023b), with a truthful response rate $r_k \in (0, 1]$. Specifically, the mechanism allows each local client to either return a true gradient with probability r_k or a synthetic Bernoulli random variable with probability $1 - r_k$. This iterative mechanism ensures

ϵ_k-LDP, where the privacy parameter is given by $\epsilon_k = \log(1+r_k) - \log(1-r_k)$, as established in Liu et al. (2023b). Combined with local SGD, the complete procedure is summarized in Algorithm 1, and we denote the resulting estimator as $\widehat{Q}_T$. By direct composition properties, Algorithm enjoys $(\max_{1 \le k \le K} \epsilon_k, 0)$-LDP guarantees.

Algorithm 1: Federated quantile estimation with local SGD under LDP

Input: step sizes $\{\eta_m\}_{m=0}^T$, target quantile $\tau \in (0, 1)$, truthful response rates $\{r_k\}_{k=1}^K$, communication set $\mathcal{I} = \{t_0, t_1, \ldots, t_T\}$.

Initialization: set $q_0^k = q_0 \sim \mathcal{N}(0, 1)$ for all $1 \le k \le K$, let $\widehat{Q}_0 \leftarrow 0$.

 for $m = 1$ to T **do**
  for $k = 1$ to K (distributedly) **do**
   for $t = t_{m-1} + 1$ to t_m **do**   ▷ Local updates
    $u_t^k \sim Bernoulli(r_k), \quad v_t^k \sim Bernoulli(0.5)$
    $s_t^k = \mathbb{I}(x_t^k > q_{t-1}^k)\mathbb{I}(u_t^k = 1) + v_t^k\mathbb{I}(u_t^k = 0)$
    $q_t^k \leftarrow q_{t-1}^k + \dfrac{1 - r_k + 2\tau r_k}{2r_k}\eta_{m-1}\mathbb{I}(s_t^k = 1) - \dfrac{1 + r_k - 2\tau r_k}{2r_k}\eta_{m-1}\mathbb{I}(s_t^k = 0)$
   end for
  end for
  $\bar{q}_{t_m} \leftarrow \sum_{k=1}^K p_k q_{t_m}^k; \, q_{t_m}^k \leftarrow \bar{q}_{t_m}$ for all $1 \le k \le K$. ▷ Aggregation and synchronization.
  $\widehat{Q}_m \leftarrow \{(m - 1)\widehat{Q}_{m-1} + \bar{q}_{t_m}\}/m$.
 end for
Return: $\widehat{Q}_T$.

In Algorithm 1, each iteration integrates global information (the global quantile τ) with client-specific data x_t^k and corresponding privacy budget (r_k), thereby correcting bias arising from the aggregation of heterogeneous local LDP mechanisms and loss functions.

Theorem 2.1. *Denote $\widetilde{\tau}_k = r_k\tau + (1 - r_k)/2$. For a privacy budget $\epsilon_k = \log(1+r_k) - \log(1-r_k)$, there exists a dataset consisting of i.i.d. samples drawn from some distribution $\widetilde{\mathcal{P}}_k, 1 \le k \le K$, such that solving the federated loss (2.1) with ϵ_k-LDP using data drawn from $\mathcal{P}_k$ for client k, is equivalent to solving the following non-private problem:*

$$Q^\star = \arg\min_Q \mathcal{L}(Q) = \arg\min_Q \widetilde{\mathcal{L}}(Q) \stackrel{\text{def}}{=} \arg\min_Q \sum_{k=1}^K \frac{p_k}{r_k} \mathbb{E}_{x_k \sim \widetilde{\mathcal{P}}_k} \left\{ \ell_{\widetilde{\tau}_k}(x_k, Q) \right\}. \tag{2.3}$$

By Theorem 2.1, federated quantile estimation via (2.1) with LDP data drawn from $\{\mathcal{P}_k\}_{k=1}^K$ can be reformulated as federated quantile estimation with non-DP data drawn from modified distributions $\{\widetilde{\mathcal{P}}_k\}_{k=1}^K$ and shifted quantile levels, as in (2.3). Consequently, the target value $Q^\star$ can be treated as the minimizer of $\widetilde{\mathcal{L}}(Q)$, a non-DP objective. The main challenge reduces to analyzing the statistical properties of the resulting non-DP estimator (under the ideal data from $\{\widetilde{\mathcal{P}}_k\}_{k=1}^K$), particularly in the presence of the non-smooth quantile loss function. Once such properties are established, the LDP inference theory can be translated directly from the relation between $(\{\mathcal{P}_k\}_{k=1}^K, \tau)$ and $(\{\widetilde{\mathcal{P}}_k\}_{k=1}^K, \{\widetilde{\tau}_k\}_{k=1}^K)$.

3 ASYMPTOTIC ANALYSIS

In this section, we focus on the asymptotic analysis of the proposed LDP estimator and the practical construction of confidence intervals. Due to the space limit, the complete assumptions and corresponding comments are provided in Appendix A.2.

Theorem 3.1. *Under Assumptions S.1-S.3, as $T \to \infty$, the proposed LDP federated estimator enjoys*

$$\sqrt{t_T}(\widehat{Q}_T - Q^\star) \xrightarrow{d} N\left(0, \nu\frac{\sum_{k=1}^K p_k^2 \left\{r_k^{-2} - (2Q_k - 1)^2\right\}}{4\left\{\sum_{k=1}^K p_k f_k(Q^\star)\right\}^2}\right).$$

Theorem 3.1 establishes the asymptotic normality of the estimator $\widehat{Q}_T$. It follows that the convergence rate of $\widehat{Q}_T$ is of order $(\min_{1 \leq k \leq K} r_k \, t_T)^{-1/2}$. Recall that the proposed algorithm satisfies $(\max_{1 \leq k \leq K} \log\{(1+r_k)/(1-r_k)\}, 0)$-LDP. which implies that the overall rate is determined by the client with the largest privacy budget. Smaller values of r_k correspond to stronger privacy protection but inevitably yield poorer estimation accuracy. If there exists any $r_k = 0$, the variance diverges and the estimator becomes inconsistent. In contrast, if all $r_k = 1$, the result recovers the classical non-DP asymptotic normality. This highlights the fundamental privacy–accuracy trade-off inherent in the proposed estimator.

Theorem 3.1 allows for the theoretical construction of a confidence interval for $Q^\star$. However, the construction involves unknown quantities, such as the individual quantiles Q_k and the density values $f_k(Q^\star)$. Even in cases where Q_k is known, the estimation of $f_k(Q^\star)$ remains challenging. In particular, it is difficult to recover these density values using only the perturbed gradients available from Algorithm 1. Moreover, in SGD-based methods, consistent variance estimation typically relies on the Hessian matrix, which is well-defined only for smooth loss functions, as previously discussed. Therefore, although Theorem 3.1 provides a theoretically valid basis for confidence interval construction, it is not practically implementable due to these limitations.

To address this issue, we establish a functional central limit theorem (FCLT) in Theorem 3.2, which serves as the foundation for constructing pivotal statistics via self-normalization (Liu et al., 2023b). This allows us to conduct inference without estimating nuisance parameters, thereby providing a direct motivation for strengthening the asymptotic result.

Theorem 3.2. *Under Assumptions S.1–S.3, as $T \to \infty$, we have*

$$\mathcal{Q}_T(s) := \frac{\sqrt{t_T}}{T} \sum_{m=1}^{h(s,T)} (\bar{q}_{t_m} - Q^\star) \xrightarrow{d} \frac{\sqrt{\nu \sum_{k=1}^{K} p_k^2 \left\{ r_k^{-2} - (2Q_k - 1)^2 \right\}}}{2 \sum_{k=1}^{K} p_k f_k(Q^\star)} B(s),$$

where $t_T = \sum_{m=0}^{T-1} E_m$, $\bar{q}_{t_m} = \sum_{k=1}^{K} p_k q_{t_m}^k$, $B(\cdot)$ is a standard Brownian motion on $[0,1]$, and

$$h(s,T) = \max \left\{ n \in \mathbb{Z}_{>0} \,\middle|\, s \sum_{m=1}^{T} \frac{1}{E_m} \geq \sum_{m=1}^{n} \frac{1}{E_m} \right\}, \quad \text{for } s \in (0,1].$$

Theorem 3.2 establishes a FCLT for $Q_T(s)$ over $s \in (0,1]$, showing that it converges weakly in the $\ell^\infty[0,1]$ (the space of bounded real-valued functions) to a Brownian motion, which is our another major theoretical contribution. Note that the sample quantile loss doesn't satisfy the common L-average smooth conditions for weakly convergence result, such in (Li et al., 2022; Xie et al., 2024; Zhu et al., 2024), leading to extra challenge in deriving the almost sure and $\mathcal{L}^2$ convergence rates of $\bar{q}_{t_m}$, which are essential for handling the asymptotically negligible terms. Theorem 3.1 arises as a special case of Theorem 3.2 when $s = 1$. Building on Theorem 3.2, we proceed to construct a self-normalized test statistic and derive its asymptotic pivotal distribution via the continuous mapping theorem.

Define $r_0 = 0$ and, for $m \geq 1$, $r_m = \left(\sum_{i=1}^{m} 1/E_i \right) \left(\sum_{i=1}^{T} 1/E_i \right)^{-1}$, which ensures that

$$\mathcal{Q}_T(r_m) = \frac{\sqrt{t_T}}{T} \sum_{i=1}^{m} (\bar{q}_{t_i} - Q^\star), \quad \text{and in particular,} \quad \mathcal{Q}_T(1) = \frac{\sqrt{t_T}}{T} \sum_{i=1}^{T} (\bar{q}_{t_i} - Q^\star).$$

Following the arguments in (Shao, 2015), once a functional central limit theorem such as Theorem 3.2 is established, one can construct a self-normalized statistic that asymptotically enjoys a pivotal distribution. Specifically, define

$$\mathcal{V}_T = \sum_{m=1}^{T} (r_m - r_{m-1}) \left\{ \mathcal{Q}_T(r_m) - \frac{m}{T} \mathcal{Q}_T(1) \right\}^2. \tag{3.1}$$

Corollary 3.1. *Suppose Assumptions S.1-S.3 hold and $g(r_m) \asymp m/T$ for some continuous function g on $[0,1]$. Then, as $T \to \infty$,*

$$\frac{\mathcal{Q}_T(1)}{\sqrt{\mathcal{V}_T}} \xrightarrow{d} \frac{B(1)}{\sqrt{\int_0^1 \left\{ B(r) - g(r) B(1) \right\}^2 dr}}.$$

Corollary 3.1 presents the asymptotic distribution of the self-normalized statistic $Q_T(1)/\mathcal{V}_T$, which is distribution-free. As a result, there is no need to allocate additional DP budget to estimate nuisance parameters when constructing confidence intervals.

The selection of the self-normalizer is not unique, and an appropriate norm of the Gaussian process $B(r) - g(r)B(1)$ can yield similar results to those in Corollary 3.1. For example, using the supremum norm and the $\mathcal{L}_1$ norm, one can define alternative self-normalizers as follows:

$$\mathcal{V}_T' = \sup_{1 \leq m \leq T} \left| \mathcal{Q}_T(r_m) - \frac{m}{T}\mathcal{Q}_T(1) \right|, \quad \mathcal{V}_T'' = \sum_{m=1}^{T} (r_m - r_{m-1}) \left| \mathcal{Q}_T(r_m) - \frac{m}{T}\mathcal{Q}_T(1) \right|,$$

which are related to the processes $\sup_{0 \leq r \leq 1} |B(r) - g(r)B(1)|$ and $\int_0^1 |B(r) - g(r)B(1)|\,dr$, respectively. However, the self-normalizer defined in equation (3.1) enjoys greater computational efficiency, as the $\mathcal{L}_2$ norm can be computed in an online manner, as described in Algorithm 2. Let $\widehat{\mathcal{V}}_T$ denote the estimator of the self-normalizer in (3.1), and let $v_{\alpha/2,g}$ be the $(1 - \alpha/2)$ quantile of the random variable $B(1)/\left[\int_0^1 \{B(r) - g(r)B_1(1)\}^2\,dr \right]^{1/2}$. The following corollary ensures the asymptotic validity of the constructed LDP confidence interval.

The following corollary ensures the asymptotic validity of the constructed LDP confidence interval.

Corollary 3.2. *Suppose the same conditions in Theorem 3.2 hold, as $T \to \infty$, one has that*

$$\mathbb{P}\left(\widehat{Q}_T - v_{\frac{\alpha}{2},g}\sqrt{\widehat{\mathcal{V}}_T} \leq Q^\star \leq \widehat{Q}_T + v_{\frac{\alpha}{2},g}\sqrt{\widehat{\mathcal{V}}_T} \right) \to 1 - \alpha$$

Algorithm 2: Online Inference

Input: step sizes $\{\eta_m\}_{m=1}^{T}$, target quantile $\tau \in (0,1)$, truthful response rates $\{r_k\}_{k=1}^{K}$, communication set $\mathcal{I} = \{t_0, t_1, \ldots, t_T\}$.

Initialization: set $q_0^k \sim \mathcal{N}(0,1)$ for all k, let $\mathcal{V}_0^a \leftarrow 0$, $\mathcal{V}_0^b \leftarrow 0$, $\mathcal{V}_0^s \leftarrow 0$, $\mathcal{V}_0^p \leftarrow 0$, and $Q_0 \leftarrow 0$.

   for $m = 1$ to T **do**

      Obtain $\widehat{Q}_m$ from Algorithm 1.

      $\mathcal{V}_m^a \leftarrow \mathcal{V}_{m-1}^a + m^2 Q_m^2/E_m,$ $\mathcal{V}_m^b \leftarrow \mathcal{V}_{m-1}^b + m^2 Q_m/E_m,$ $\triangleright\ E_m = t_m - t_{m-1}$

      $\mathcal{V}_m^s \leftarrow \mathcal{V}_{m-1}^s + 1/E_m$ $\mathcal{V}_m^p \leftarrow \mathcal{V}_{m-1}^p + m^2/E_m.$

      $\widehat{\mathcal{V}}_m \leftarrow \frac{1}{m^2 \mathcal{V}_m^s}\left(\mathcal{V}_m^a - 2\mathcal{V}_m^b Q_m + \mathcal{V}_m^p Q_m^2 \right).$ $\triangleright$ Online inference.

   end for

Return: Confidence interval $\left[\widehat{Q}_T - v_{\frac{\alpha}{2},g}\sqrt{\widehat{\mathcal{V}}_T}, \ \ \widehat{Q}_T + v_{\frac{\alpha}{2},g}\sqrt{\widehat{\mathcal{V}}_T} \right].$

---

4 EXPERIMENTS

4.1 SIMULATION SETUP

We first evaluate our proposed method through extensive simulation studies using synthetic data. In all experiments, we fixed $p_k = 1/K$ for $1 \leq k \leq K$, the number of clients is fixed at $K = 10$. The quantile levels examined range from 0.3 to 0.8, and the truthful response rates vary between 0.25 and 0.9. We focus on the following four scenarios of heterogeneity:

- **heterogeneous quantile levels:** We investigate two distinct scenarios: (1) Case τ_{low}: lower quantile levels, where each client is assigned a unique quantile level τ_k ranging uniformly from 0.3 to 0.5; and (2) Case τ_{high}: higher quantile levels, where τ_k ranges uniformly from 0.5 to 0.8.

- **heterogeneous response rates.** Each client has a unique truthful response rate r_k, ranging uniformly from 0.25 to 0.9.

- **heterogeneous locations (Hete L).** Data for each client k are independently generated from $\mathcal{N}(\mu_k, 1)$ or $\mathcal{C}(\mu_k, 1)$, where $\mu_k \sim \mathcal{N}(0,1)$.

- **heterogeneous distribution families (Hete D).** Data are generated independently across ten clients, with three drawing from $\mathcal{N}(0,1)$, three from the uniform distribution $\mathcal{U}(-1,1)$, and four from a standard Cauchy distribution $\mathcal{C}(0,1)$.

We set the step size γ_m as: $\gamma_m = 20\bar{r}/(m^{0.51} + 100)$, with $\gamma_m = E_m \eta_m$ and $\bar{r} = K^{-1} \sum_{k=1}^{K} r_k$. Following Li et al. (2022), we implement a warm-up phase, setting the communication interval $E_m = 1$ for the first 5% of iterations. After the warm-up period, we redefine the interval sequence $\{E_m\}$ based on a new sequence $\{E'_m\}$, specifically: $E_m = E'_{m-0.05 \cdot T}$. We examine three different interval strategies for E'_m: (1) C1: $E'_m \equiv 1$ (equivalent to parallel SGD), (2) C5: $E'_m \equiv 5$, and (3) Log: $E'_m = \lceil \log_2(m+1) \rceil$. The initial parameter estimates are set to $q_0^k = q_0 \sim \mathcal{N}(0,1)$ for all clients k. All experimental settings are replicated $R = 1,000$ times. The simulations are conducted on computational resources comprising 36 Intel Xeon Gold 6271 CPUs, with a total of 128GB RAM and 500GB storage.

4.2 Simulation results

We first illustrate the performance of our proposed method by presenting sample iteration trajectories for estimation and inference. Specifically, we randomly select one simulation run and plot the resulting estimates and corresponding confidence intervals against t_T (Figure S.1). The results demonstrate that our approach accurately captures the true quantile value and provides reliable inference. Subsequently, we fix t_T at $10,000$ and $50,000$ and evaluate the finite sample performance under different settings. Let $\widehat{Q}_T^{(r)}$ denote the quantile estimator and $\mathrm{CI}^{(r)}$ represent the corresponding 95% confidence interval obtained from Algorithm 2 in the r-th simulation. We consider two metrics: the mean absolute error (MAE), defined as $R^{-1} \sum_{r=1}^{R} |\widehat{Q}_T^{(r)} - Q^*|$, and the empirical coverage probability (ECP), defined as $R^{-1} \sum_{r=1}^{R} \mathbb{I}(Q^* \in \mathrm{CI}^{(r)})$. For comparison, we also consider two alternative methods: (1) the SGD with DP updates (Song et al., 2013) (DP-SGD), which adds noise directly to the gradients instead of introducing DP through randomized response. To align with the original paper's setup, we focus on the case with $C = 1$. In this regime, the gradient-descent update in Algorithm 1 becomes

$$q_t^k \leftarrow q_{t-1}^k + \eta_{t-1} \Big\{ \tau_k \mathbb{I}(x_t^k > q_{t-1}^k) - (1 - \tau_k) \mathbb{I}(x_t^k < q_{t-1}^k) + Z_t^k \Big\},$$

where Z_t^k is drawn from a Laplace distribution. A simple calculation shows that Z_t^k has mean zero and scale parameter $1/\log\{(1 + r_k)/(1 - r_k)\}$. (2) the divide-and-conquer (DC) method, which corresponds to the special case $E_m = t_T$. Here we use step size $\eta_t = 2\bar{r}/(t^{0.51} + 100)$ (Goyal et al., 2017). (3) the single-machine LDP quantile inference method (Single) (Liu et al., 2023b), where all data hold on a single device and LDP-SGD is performed without any federated communication. The numerical results for all methods under the normal distribution setting are reported in Tables 1 and 2, while the corresponding results under the Cauchy distribution setting are summarized in Tables S.2 and S.3.

From the results, we observe that our method consistently achieves ECP close to or exceeding the nominal 95% level across all scenarios, and that the C1 strategy (parallel SGD) performs essentially comparably to the Single baseline. As either the total sample size t_T or the truthful response rate increases, the MAE decreases, which aligns with our theoretical results. Comparing the three interval strategies, we find that the C1 strategy yields the smallest MAE, as it has the highest communication frequency. Comparing with the two competing methods, we find that the DC approach results in the largest errors. Notably, in certain heterogeneous cases, such as Hete L with $\tau = 0.8$, the DC estimator exhibits significant bias and an ECP far below the nominal 95% level. In contrast, our proposed estimators successfully achieve approximately 95% empirical coverage in these cases. Moreover, while DP-SGD attains empirical coverage probabilities close to or even exceeding 95% in most settings, its MAE remain uniformly larger than those of our method.

To further illustrate the efficiency–accuracy trade-off of our method, we conduct a quantitative analysis in which we record the wall-clock time; the results are shown in Figure S.2 in Appendix C.1. We also consider scenarios with a fixed number of communication rounds T, with the corresponding results summarized in Tables S.4 and S.5 in Appendix C.1. We observe that our proposed method continues to provide valid inference. Additionally, under fixed communication rounds, the Log strategy generally achieves the best performance, yielding the smallest MAE.

Quantile (τ)	Rate (r)	C1	C5	Log	DP-SGD (C1)	DC	Single
			Hete L — $t_T = 10000$				
0.3	0.25	0.958(0.0184)	0.981(0.0311)	0.990(0.0452)	0.942(0.0260)	0.985(0.3066)	0.950(0.0222)
0.3	hetero	0.949(0.0096)	0.982(0.0150)	0.993(0.0205)	0.947(0.0142)	0.898(0.1302)	0.954(0.0095)
0.3	0.9	1.000(0.0029)	1.000(0.0066)	1.000(0.0100)	0.981(0.0049)	0.215(0.1273)	0.962(0.0055)
0.5	0.25	0.950(0.0165)	0.984(0.0315)	0.988(0.0465)	0.953(0.0224)	1.000(0.2822)	0.930(0.0192)
0.5	hetero	0.952(0.0085)	0.991(0.0155)	0.998(0.0221)	0.955(0.0119)	1.000(0.0525)	0.952(0.0083)
0.5	0.9	0.996(0.0025)	0.999(0.0078)	1.000(0.0120)	0.984(0.0041)	1.000(0.0186)	0.952(0.0051)
0.8	0.25	0.966(0.0237)	0.995(0.0512)	0.992(0.0791)	0.957(0.0328)	0.892(0.6152)	0.942(0.0277)
0.8	hetero	0.962(0.0122)	0.995(0.0227)	0.996(0.0347)	0.943(0.0186)	0.709(0.2684)	0.958(0.0114)
0.8	0.9	0.990(0.0042)	1.000(0.0116)	1.000(0.0185)	0.968(0.0065)	0.049(0.2098)	0.966(0.0067)
			Hete L — $t_T = 50000$				
0.3	0.25	0.937(0.0089)	0.981(0.0111)	0.990(0.0165)	0.916(0.0135)	0.949(0.1328)	0.948(0.0095)
0.3	hetero	0.911(0.0056)	0.981(0.0056)	0.997(0.0080)	0.885(0.0083)	0.093(0.1282)	0.958(0.0038)
0.3	0.9	0.977(0.0034)	1.000(0.0019)	1.000(0.0030)	0.908(0.0041)	0.000(0.1290)	0.938(0.0024)
0.5	0.25	0.958(0.0069)	0.988(0.0098)	0.995(0.0147)	0.949(0.0099)	1.000(0.0609)	0.940(0.0082)
0.5	hetero	0.964(0.0035)	0.994(0.0048)	0.996(0.0069)	0.957(0.0052)	0.997(0.0145)	0.938(0.0034)
0.5	0.9	1.000(0.0010)	1.000(0.0016)	1.000(0.0026)	0.993(0.0018)	0.979(0.0143)	0.950(0.0022)
0.8	0.25	0.956(0.0102)	0.991(0.0144)	0.998(0.0226)	0.931(0.0160)	0.799(0.2829)	0.954(0.0114)
0.8	hetero	0.950(0.0055)	0.992(0.0072)	0.997(0.0112)	0.923(0.0092)	0.014(0.2034)	0.952(0.0046)
0.8	0.9	1.000(0.0013)	1.000(0.0053)	0.999(0.0082)	0.985(0.0026)	0.000(0.1929)	0.950(0.0027)
			Hete D — $t_T = 10000$				
0.5	0.25	0.949(0.0132)	0.985(0.0243)	0.986(0.0354)	0.953(0.0183)	0.904(0.2496)	0.936(0.0139)
0.5	hetero	0.966(0.0069)	0.990(0.0117)	0.989(0.0172)	0.955(0.0098)	0.999(0.0488)	0.958(0.0057)
0.5	0.9	1.000(0.0023)	1.000(0.0074)	1.000(0.0117)	0.991(0.0035)	1.000(0.0163)	0.946(0.0037)
			Hete D — $t_T = 50000$				
0.5	0.25	0.958(0.0057)	0.980(0.0082)	0.993(0.0127)	0.943(0.0081)	0.981(0.0589)	0.940(0.0058)
0.5	hetero	0.966(0.0030)	0.988(0.0046)	0.998(0.0073)	0.950(0.0041)	1.000(0.0111)	0.958(0.0025)
0.5	0.9	0.999(0.0008)	1.000(0.0029)	1.000(0.0052)	0.990(0.0014)	1.000(0.0037)	0.950(0.0016)

Table 1: Empirical coverage probabilities at the 95% nominal level (mean absolute errors ↓) under heterogeneous distributions for different t_T. The number of clients K is fixed at 10. In Hete L, data for each client k are independently generated from $\mathcal{N}(\mu_k, 1)$, where $\mu_k \sim \mathcal{N}(0, 1)$. In Hete D, data are generated from $\mathcal{N}(0, 1)$, $\mathcal{U}(-1, 1)$, and $\mathcal{C}(0, 1)$ across different clients. "hetero" indicates client-specific truthful response rates r_k range uniformly from $[0.25, 0.9]$.

Quantile (τ)	Rate (r)	C1	C5	Log	DP-SGD (C1)	DC	Single
				$t_T = 10000$			
0.5	0.25	0.949(0.0133)	0.967(0.0244)	0.992(0.0360)	0.949(0.0191)	0.939(0.2503)	0.934(0.0141)
0.5	hetero	0.963(0.0071)	0.989(0.0112)	0.997(0.0161)	0.955(0.0100)	1.000(0.0497)	0.956(0.0059)
0.5	0.9	0.995(0.0023)	1.000(0.0054)	1.000(0.0082)	0.980(0.0036)	1.000(0.0158)	0.950(0.0039)
τ_{low}	0.25	0.947(0.0136)	0.982(0.0253)	0.990(0.0369)	0.940(0.0200)	0.969(0.2616)	0.950(0.0141)
τ_{low}	hetero	0.962(0.0072)	0.993(0.0113)	0.997(0.0162)	0.949(0.0105)	0.999(0.0530)	0.946(0.0063)
τ_{low}	0.9	0.999(0.0020)	1.000(0.0055)	1.000(0.0083)	0.985(0.0036)	1.000(0.0162)	0.942(0.0040)
τ_{high}	0.25	0.939(0.0145)	0.987(0.0268)	0.986(0.0399)	0.952(0.0210)	0.984(0.2771)	0.930(0.0152)
τ_{high}	hetero	0.968(0.0076)	0.987(0.0126)	0.999(0.0182)	0.956(0.0111)	1.000(0.0516)	0.972(0.0061)
τ_{high}	0.9	0.996(0.0023)	1.000(0.0067)	1.000(0.0102)	0.980(0.0038)	1.000(0.0172)	0.962(0.0039)
				$t_T = 50000$			
0.5	0.25	0.956(0.0056)	0.982(0.0081)	0.996(0.0122)	0.949(0.0081)	0.988(0.0571)	0.952(0.0058)
0.5	hetero	0.960(0.0032)	0.979(0.0044)	0.992(0.0064)	0.950(0.0046)	1.000(0.0115)	0.960(0.0025)
0.5	0.9	1.000(0.0018)	0.988(0.0027)	0.990(0.0036)	0.983(0.0021)	1.000(0.0038)	0.950(0.0016)
τ_{low}	0.25	0.957(0.0061)	0.981(0.0083)	0.994(0.0125)	0.944(0.0091)	0.993(0.0594)	0.944(0.0059)
τ_{low}	hetero	0.953(0.0036)	0.981(0.0054)	0.990(0.0066)	0.934(0.0053)	0.999(0.0121)	0.962(0.0026)
τ_{low}	0.9	1.000(0.0019)	1.000(0.0026)	0.989(0.0038)	0.988(0.0024)	1.000(0.0057)	0.958(0.0017)
τ_{high}	0.25	0.968(0.0059)	0.986(0.0086)	0.997(0.0133)	0.946(0.0089)	0.999(0.0620)	0.944(0.0061)
τ_{high}	hetero	0.953(0.0032)	0.990(0.0045)	0.998(0.0065)	0.952(0.0047)	0.993(0.0154)	0.948(0.0028)
τ_{high}	0.9	0.998(0.0010)	0.999(0.0023)	1.000(0.0034)	0.977(0.0016)	0.938(0.0132)	0.958(0.0017)

Table 2: Empirical coverage probabilities at the 95% nominal level (mean absolute errors ↓) under varying quantile levels and response rates, with different t_T and fixed $K = 10$ clients and data generated from $\mathcal{N}(0, 1)$. In Case τ_{low}, each client uses a unique quantile level τ_k ranging uniformly from $[0.3, 0.5]$; in Case τ_{high}, τ_k is ranging from $[0.5, 0.8]$. "hetero" indicates client-specific truthful response rates r_k range uniformly from $[0.25, 0.9]$.

Finally, to further strengthen our simulation study, we conducted a set of additional experiments, including: (1) consider partial client participation to mimic more realistic federated environments; (2) sensitivity analyses on the truthful response rate and step-size schedule to assess the robustness of the method; (3) a comparison between the resulting confidence intervals and oracle normal-based intervals to illustrate the conservativeness of the self-normalized inference procedure; and (4) an initial exploration of extending our method to a fully decentralized federated learning setting; see Appendix C for details.

4.3 REAL DATA

In this subsection, we empirically evaluate the effectiveness of our proposed method using a representative real-world dataset widely employed in privacy research: Government Salary Dataset (Plečko et al., 2024). This dataset is sourced from the 2018 American Community Survey conducted by the U.S. Census Bureau and contains over 200,000 records, with annual salary (in USD) as the response variable. Since annual salary represents sensitive financial information (Gillenwater et al., 2021), we treat it as requiring privacy protection. To incorporate the dataset's inherent geographic structure, we partition the sample according to the feature "economic region." The three smallest regions are merged into a single "Others" category, yielding seven regions in total, each regarded as one client. Because region-level sample sizes vary, we apply oversampling to balance the data, resulting in $t_T = 53,960$ observations per client. All other hyperparameters follow the settings in Section 4.1. For analysis, we apply a log transformation to the response variable and subsequently back-transform it.

We target quantile levels $\tau_k \equiv \tau \in \{0.3, 0.5, 0.8\}$ and consider response rates $r_k \in \{0.6, \text{hetero}, 0.9\}$, where "hetero" indicates client-specific truthful response rates r_k range uniformly from 0.6 to 0.9. For reference, we also compute the full-sample quantiles without LDP. The resulting estimators and confidence-interval lengths are summarized in Table 3. As shown, higher response rates r and more communication rounds generally produce shorter confidence intervals, consistent with our simulation findings. In most cases, the empirical quantiles fall within our reported intervals, highlighting the practical utility of our method for real data.

Quantile (τ)	Rate (r)	C1	C5	Log	Empirical
0.3	0.6	33367 (1742)	33184 (6697)	33030 (12093)	
0.3	hetero	33418 (1424)	33229 (5291)	33140 (9788)	34000
0.3	0.9	33547 (1548)	33403 (4443)	33239 (7828)	
0.5	0.6	48454 (2255)	48212 (6315)	47951 (11361)	
0.5	hetero	48462 (1435)	48290 (4973)	48091 (9025)	50000
0.5	0.9	48610 (1454)	48494 (3851)	48311 (6863)	
0.8	0.6	78586 (2066)	78168 (6646)	77995 (13144)	
0.8	hetero	78390 (1291)	78054 (5862)	77722 (11101)	80000
0.8	0.9	78657 (1138)	78300 (4677)	78084 (8928)	

Table 3: Estimation results (interval lengths) on the real dataset across varying quantile levels and response rates. "Empirical" denotes the full-sample quantile estimator without LDP. "hetero" indicates client-specific truthful response rates r_k range uniformly from 0.6 to 0.9.

5 CONCLUDING REMARK

We propose a federated-learning algorithm for quantile inference under LDP that flexibly accommodates client-level heterogeneity in quantile targets, privacy budgets, and data distributions. In addition, one innovation that should be emphasized is that our developed theoretical results of local SGD quantile estimator. We first design an LDP mechanism that can transform the LDP federated quantile estimation into the non-DP case, and then derive the asymptotic normality and functional central limit theorem of the proposed estimator under non-DP cases. It is first weak-convergence result for local SGD without the usual average-smoothness assumption in existing literature. Building on these non-private asymptotic results, we develop a self-normalized inference procedure that constructs valid confidence intervals under LDP without requiring direct estimation of variance.

Despite these advances, our method has several limitations. First, it relies on additional regularity assumptions to handle arbitrary client-level data heterogeneity. Second, as noted in (Shao, 2015), self-normalization yields heavier-tailed limit distributions than the Gaussian, which can produce conservative confidence intervals or reduced power in hypothesis testing. In addition, theoretically understanding how asynchronous or partial client participation affects estimation and inference is also an important direction for future work. Finally, our framework depends on a central server for aggregation and synchronization, which may not be available in fully decentralized environments. Addressing these challenges and extending the algorithm to decentralized settings remain important directions for future research.

ACKNOWLEDGMENTS

REPRODUCIBILITY STATEMENT

All numerical experiments and real-data analyses are fully reproducible via the code included in the supplementary materials.

REFERENCES

Naman Agarwal, Ananda Theertha Suresh, Felix Xinnan X Yu, Sanjiv Kumar, and Brendan McMahan. cpsgd: Communication-efficient and differentially-private distributed sgd. *Advances in Neural Information Processing Systems*, 31, 2018.

Joshua Angrist, Victor Chernozhukov, and Iván Fernández-Val. Quantile regression under misspecification, with an application to the us wage structure. *Econometrica*, 74(2):539–563, 2006.

Luca Barbaglia, Sergio Consoli, and Sebastiano Manzan. Forecasting with economic news. *Journal of Business & Economic Statistics*, 41(3):708–719, 2023.

Steven Bellman, Eric J Johnson, Stephen J Kobrin, and Gerald L Lohse. International differences in information privacy concerns: A global survey of consumers. *The Information Society*, 20(5): 313–324, 2004.

T Tony Cai, Yichen Wang, and Linjun Zhang. The cost of privacy: Optimal rates of convergence for parameter estimation with differential privacy. *The Annals of Statistics*, 49(5):2825–2850, 2021.

Likai Chen, Georg Keilbar, and Wei Biao Wu. Recursive quantile estimation: Non-asymptotic confidence bounds. *Journal of Machine Learning Research*, 24(91):1–25, 2023.

Song Xi Chen. Nonparametric estimation of expected shortfall. *Journal of financial econometrics*, 6(1):87–107, 2008.

Xi Chen, Jason D Lee, Xin T Tong, and Yichen Zhang. Statistical inference for model parameters in stochastic gradient descent. *The Annals of Statistics*, 48(1):251–273, 2020.

Xi Chen, Weidong Liu, and Yichen Zhang. First-order newton-type estimator for distributed estimation and inference. *Journal of the American Statistical Association*, 117(540):1858–1874, 2022.

Victor Chernozhukov and Iván Fernández-Val. Inference for extremal conditional quantile models, with an application to market and birthweight risks. *The Review of Economic Studies*, 78(2): 559–589, 2011.

Victor Chernozhukov and Christian Hansen. An iv model of quantile treatment effects. *Econometrica*, 73(1):245–261, 2005.

Albert Cheu, Adam Smith, Jonathan Ullman, David Zeber, and Maxim Zhilyaev. Distributed differential privacy via shuffling. In *Advances in Cryptology–EUROCRYPT 2019: 38th Annual International Conference on the Theory and Applications of Cryptographic Techniques, Darmstadt, Germany, May 19–23, 2019, Proceedings, Part I 38*, pp. 375–403. Springer, 2019.

Bolin Ding, Janardhan Kulkarni, and Sergey Yekhanin. Collecting telemetry data privately. *Advances in Neural Information Processing Systems*, 30, 2017.

John C Duchi, Michael I Jordan, and Martin J Wainwright. Local privacy and statistical minimax rates. In *2013 IEEE 54th Annual Symposium on Foundations of Computer Science*, pp. 429–438. IEEE, 2013.

Cynthia Dwork, Krishnaram Kenthapadi, Frank McSherry, Ilya Mironov, and Moni Naor. Our data, ourselves: Privacy via distributed noise generation. In *Annual International Conference on the Theory and Applications of Cryptographic Techniques*, pp. 486–503. Springer, 2006.

Úlfar Erlingsson, Vasyl Pihur, and Aleksandra Korolova. Rappor: Randomized aggregatable privacy-preserving ordinal response. In *Proceedings of the 2014 ACM SIGSAC conference on computer and communications security*, pp. 1054–1067, 2014.

Jennifer Gillenwater, Matthew Joseph, and Alex Kulesza. Differentially private quantiles. In Marina Meila and Tong Zhang (eds.), *Proceedings of the 38th International Conference on Machine Learning*, volume 139 of *Proceedings of Machine Learning Research*, pp. 3713–3722. PMLR, 18–24 Jul 2021.

Priya Goyal, Piotr Dollár, Ross Girshick, Pieter Noordhuis, Lukasz Wesolowski, Aapo Kyrola, Andrew Tulloch, Yangqing Jia, and Kaiming He. Accurate, large minibatch sgd: Training imagenet in 1 hour. *arXiv preprint arXiv:1706.02677*, 2017.

Jia Gu and Song Xi Chen. Distributed statistical inference under heterogeneity. *Journal of Machine Learning Research*, 24(387):1–57, 2023.

Peter Hall and Christopher C Heyde. *Martingale limit theory and its application*. Academic press, 2014.

Xuming He, Xiaoou Pan, Kean Ming Tan, and Wen-Xin Zhou. Smoothed quantile regression with large-scale inference. *Journal of Econometrics*, 232(2):367–388, 2023.

Jiaqiao Hu, Yijie Peng, Gongbo Zhang, and Qi Zhang. A stochastic approximation method for simulation-based quantile optimization. *INFORMS Journal on Computing*, 34(6):2889–2907, 2022.

Jie Hu, Yi-Ting Ma, and Do-Young Eun. Does worst-performing agent lead the pack? analyzing agent dynamics in unified distributed sgd. *Advances in Neural Information Processing Systems*, 37:72754–72789, 2024.

Ziyue Huang, Yuting Liang, and Ke Yi. Instance-optimal mean estimation under differential privacy. *Advances in Neural Information Processing Systems*, 34:25993–26004, 2021.

Xue Jiang, Xuebing Zhou, and Jens Grossklags. Signds-fl: Local differentially private federated learning with sign-based dimension selection. *ACM Transactions on Intelligent Systems and Technology (TIST)*, 13(5):1–22, 2022.

Matthew Joseph, Jieming Mao, Seth Neel, and Aaron Roth. The role of interactivity in local differential privacy. In *2019 IEEE 60th Annual Symposium on Foundations of Computer Science (FOCS)*, pp. 94–105, 2019. doi: 10.1109/FOCS.2019.00015.

Nathan Kallus, Xiaojie Mao, and Masatoshi Uehara. Localized debiased machine learning: Efficient inference on quantile treatment effects and beyond. *Journal of Machine Learning Research*, 25 (16):1–59, 2024.

Jakub Konečnỳ, H Brendan McMahan, Felix X Yu, Peter Richtárik, Ananda Theertha Suresh, and Dave Bacon. Federated learning: Strategies for improving communication efficiency. *arXiv preprint arXiv:1610.05492*, 2016.

Boyuan Li, Shaohui Zhang, and Qiuying Han. Federated learning with joint server-client momentum. *Scientific Reports*, 15(1):15626, 2025.

Tian Li, Anit Kumar Sahu, Manzil Zaheer, Maziar Sanjabi, Ameet Talwalkar, and Virginia Smith. Federated optimization in heterogeneous networks. *Proceedings of Machine learning and systems*, 2:429–450, 2020.

Xiang Li, Jiadong Liang, Xiangyu Chang, and Zhihua Zhang. Statistical estimation and online inference via local sgd. In *Conference on Learning Theory*, pp. 1613–1661. PMLR, 2022.

Chun Liu, Youliang Tian, Jinchuan Tang, Shuping Dang, and Gaojie Chen. A novel local differential privacy federated learning under multi-privacy regimes. *Expert systems with applications*, 227: 120266, 2023a.

Wei Liu, Li Chen, Yunfei Chen, and Wenyi Zhang. Accelerating federated learning via momentum gradient descent. *IEEE Transactions on Parallel and Distributed Systems*, 31(8):1754–1766, 2020.

Yi Liu, Qirui Hu, Lei Ding, and Linglong Kong. Online local differential private quantile inference via self-normalization. In *International Conference on Machine Learning*, pp. 21698–21714. PMLR, 2023b.

Andrew Lowy and Meisam Razaviyayn. Private federated learning without a trusted server: Optimal algorithms for convex losses. In *The Eleventh International Conference on Learning Representations*, 2023.

Xu Ma, Xiaoqian Sun, Yuduo Wu, Zheli Liu, Xiaofeng Chen, and Changyu Dong. Differentially private byzantine-robust federated learning. *IEEE Transactions on Parallel and Distributed Systems*, 33(12):3690–3701, 2022.

Horia Mania, Xinghao Pan, Dimitris Papailiopoulos, Benjamin Recht, Kannan Ramchandran, and Michael I Jordan. Perturbed iterate analysis for asynchronous stochastic optimization. *SIAM Journal on Optimization*, 27(4):2202–2229, 2017.

Brendan McMahan, Eider Moore, Daniel Ramage, Seth Hampson, and Blaise Aguera y Arcas. Communication-efficient learning of deep networks from decentralized data. In *Artificial intelligence and statistics*, pp. 1273–1282. PMLR, 2017.

Sandra J Milberg, H Jeff Smith, and Sandra J Burke. Information privacy: Corporate management and national regulation. *Organization science*, 11(1):35–57, 2000.

Drago Plečko, Nicolas Bennett, and Nicolai Meinshausen. fairadapt: Causal reasoning for fair data preprocessing. *Journal of Statistical Software*, 110:1–35, 2024.

Herbert Robbins and David Siegmund. A convergence theorem for non negative almost super-martingales and some applications. In *Optimizing methods in statistics*, pp. 233–257. Elsevier, 1971.

Xiaofeng Shao. Self-normalization for time series: a review of recent developments. *Journal of the American Statistical Association*, 110(512):1797–1817, 2015.

Xiaoying Shen, Hang Jiang, Yange Chen, Baocang Wang, and Le Gao. Pldp-fl: Federated learning with personalized local differential privacy. *Entropy*, 25(3):485, 2023.

Siping Shi, Chuang Hu, Dan Wang, Yifei Zhu, and Zhu Han. Distributionally robust federated learning for differentially private data. In *2022 IEEE 42nd International Conference on Distributed Computing Systems (ICDCS)*, pp. 842–852. IEEE, 2022.

Shuang Song, Kamalika Chaudhuri, and Anand D Sarwate. Stochastic gradient descent with differentially private updates. In *2013 IEEE global conference on signal and information processing*, pp. 245–248. IEEE, 2013.

Sebastian U Stich. Local sgd converges fast and communicates little. *arXiv preprint arXiv:1805.09767*, 2018.

Weijie J Su and Yuancheng Zhu. Uncertainty quantification for online learning and stochastic approximation via hierarchical incremental gradient descent. *arXiv preprint arXiv:1802.04876*, 2018.

Ye Tian, Haolei Weng, and Yang Feng. Unsupervised federated learning: A federated gradient em algorithm for heterogeneous mixture models with robustness against adversarial attacks. *arXiv preprint arXiv:2310.15330*, 2023.

Huixia Judy Wang, Deyuan Li, and Xuming He. Estimation of high conditional quantiles for heavy-tailed distributions. *Journal of the American Statistical Association*, 107(500):1453–1464, 2012.

Chuhan Xie, Kaicheng Jin, Jiadong Liang, and Zhihua Zhang. Asymptotic time-uniform inference for parameters in averaged stochastic approximation. *arXiv preprint arXiv:2410.15057*, 2024.

Steve Yadlowsky, Scott Fleming, Nigam Shah, Emma Brunskill, and Stefan Wager. Evaluating treatment prioritization rules via rank-weighted average treatment effects. *Journal of the American Statistical Association*, 120(549):38–51, 2025.

Yang Zhao, Jun Zhao, Mengmeng Yang, Teng Wang, Ning Wang, Lingjuan Lyu, Dusit Niyato, and Kwok-Yan Lam. Local differential privacy-based federated learning for internet of things. *IEEE Internet of Things Journal*, 8(11):8836–8853, 2020.

Wanrong Zhu, Zhipeng Lou, Ziyang Wei, and Wei Biao Wu. High confidence level inference is almost free using parallel stochastic optimization. *arXiv preprint arXiv:2401.09346*, 2024.

A NOTATIONS AND COMPLETE ASSUMPTIONS

A.1 NOTATIONS

Notations	Meanings
$\mathcal{L}$	Global Loss function
τ	Global quantile
$\mathcal{L}_{\tau_k}$	Local loss function for client k with local quantile τ_k
p_k	the weight assigned to client k
$\mathcal{P}_k$	Distribution for client k
F_k	CDF for client k
f_k	Density function for client k
$\mathcal{I}$	Communication iteration sets
t_m	Communication iteration time
E_m	Interval length
Q	Variable in loss function
$Q^\star$	True or target value
Q_k	Value at $F_k(Q^*)$
q_{t+1}^k	Iterations at step t for client k
r_k	Response rate for for client k
ϵ_k	Privacy budget for client k
$\widehat{\mathcal{Q}}_T$	LDP federated quantile estimator
$\widehat{\mathcal{V}}_T$	LDP federated quantile self-normalizer
$B(s)$	Brownian motion
$v_{\alpha/2,g}$	$(1 - \alpha/2)$ quantile of self-normalization distribution

Table S.1: Notations table.

A.2 COMPLETE ASSUMPTIONS

We introduce the following necessary assumptions.

Assumption S.1. *For some constant $C_f > 0$, $f_k(\cdot)$, $1 \leq k \leq K$, the density function for client k, is uniformly bounded by C_f, and $\min_{1 \leq k \leq K} f_k(Q^\star) > 0$.*

Assumption S.2. *Define the effective step $\gamma_m = \eta_m E_m$, which is non-increasing in m and satisfies that $\sum_{m=1}^{\infty} \gamma_m^2 < \infty$, $\sum_{m=1}^{\infty} \gamma_m = \infty$, and $(\gamma_m - \gamma_{m+1})/\gamma_m = \mathcal{O}(\gamma_m)$.*

Assumption S.3. *The sequence $\{E_m\}_{m \geq 1}$ satisfies that*

(a) $\{E_m\}_{m \geq 1}$ is either uniformly bounded or non-decreasing.

14

(b) There exist some $\delta > 0$ and $\nu \geq 1$ such that

$$\limsup_{T \to \infty} \frac{1}{T^2} \left(\sum_{m=0}^{T-1} E_m^{1+\delta} \right) \left(\sum_{m=0}^{T-1} E_m^{-1-\delta} \right) < \infty, \quad \lim_{T \to \infty} \frac{1}{T^2} \left(\sum_{m=0}^{T-1} E_m \right) \left(\sum_{m=0}^{T-1} E_m^{-1} \right) = \nu.$$

(c) Denote $t_T = \sum_{m=0}^{T-1} E_m$, satisfying

$$\lim_{T \to \infty} \frac{\sqrt{t_T}}{T} \sum_{m=0}^{T} \gamma_m = 0, \quad \lim_{T \to \infty} \frac{\sqrt{t_T}}{T} \frac{1}{\sqrt{\gamma_T}} = 0$$

Assumption S.1 is a mild and regular condition concerning the uniform boundedness of density functions. Assumptions S.2 and S.3 require that the effective step sizes decay slowly and the communication intervals increase slowly; see also Li et al. (2022).

B TECHNIQUE PROOFS

Proof of Theorem 2.1: Note that the following recursive equation

$$q_t^k = q_{t-1}^k + \frac{1 - r_k + 2\tau r_k}{2r_k} \eta_{m-1} \mathbb{I}(s_t^k = 1) - \frac{1 + r_k - 2\tau r_k}{2r_k} \eta_{m-1} \mathbb{I}(s_t^k = 0),$$

is asymptotically equivalent to

$$q_t^k = q_{t-1}^k + \eta_{m-1} \frac{1}{r_k} \left\{ \frac{1 - r_k + 2\tau r_k}{2} - \mathbb{I}(\widetilde{x}_t^k \leq q_{t-1}^k) \right\},$$

where

$$\mathbb{P}(\widetilde{x}_t^k = x_t^k) = r_k, \quad \mathbb{P}(\widetilde{x}_t^k = \infty) = \mathbb{P}(\widetilde{x}_t^k = -\infty) = (1 - r_k)/2.$$

Observe that the above SGD update is designed to solve the following non-DP loss function

$$\arg\min_{Q_k} \mathbb{E}_{x_k \sim \widetilde{\mathcal{P}}_k} \left\{ r_k^{-1} \ell_{\widetilde{\tau}_k}(x_k, Q_k) \right\}.$$

Inspired by this, we denote

$$Q^{\spadesuit} := \arg\min_Q \sum_{k=1}^{K} p_k \mathbb{E}_{x_k \sim \widetilde{\mathcal{P}}_k} \left\{ r_k^{-1} \ell_{\widetilde{\tau}_k}(x_k, Q) \right\}$$

$$= \arg\min_Q \sum_{k=1}^{K} \frac{p_k}{r_k} \mathbb{E}_{x_k \sim \widetilde{\mathcal{P}}_k} \left[(x_k - Q) \left\{ \widetilde{\tau}_k - \mathbb{I}(x_k \leq Q) \right\} \right].$$

In the following, we desire to verify that $Q^{\spadesuit} = Q^{\star}$. By the definition of the minimizer of the objective function,

$$\sum_{k=1}^{K} \frac{p_k}{r_k} \left\{ \mathbb{P}(\widetilde{x}_t^k \leq Q^{\spadesuit}) - \widetilde{\tau}_k \right\} = 0.$$

Since $\widetilde{\tau}_k = r_k \tau + (1 - r_k)/2$, and

$$\mathbb{P}(\widetilde{x}_t^k \leq Q^{\spadesuit}) = r_k F_k(Q^{\spadesuit}) + (1 - r_k)/2,$$

one has

$$\sum_{k=1}^{K} \left\{ p_k F_k(Q^{\spadesuit}) + p_k(1 - r_k)/(2r_k) \right\} = \sum_{k=1}^{K} \left\{ p_k(1 - r_k)/(2r_k) + p_k \tau \right\}.$$

Subtracting $\sum_{k=1}^{K} \left\{ p_k(1 - r_k)/(2r_k) \right\}$ from both sides of the equation, we obtain

$$\sum_{k=1}^{K} p_k F_k(Q^{\spadesuit}) = \sum_{k=1}^{K} p_k \tau = \tau.$$

15

Recall that the definition of $\tau = \sum_{k=1}^K p_k F_k(Q^\star)$, we show that

$$\sum_{k=1}^K p_k F_k(Q^\spadesuit) = \sum_{k=1}^K p_k F_k(Q^\star),$$

which implies $Q^\spadesuit = Q^\star$. The proof is now completed.

Proof of Theorem 3.1:

Theorem 3.1 is a direct consequence of Theorem 3.2.

Proof of Theorem 3.2:

We follows the perturbed iterate framework that is derived by Mania et al. (2017) and also used in Li et al. (2022). Define the sequence $\bar{q}_t$ in the following way:

$$\bar{q}_t = \sum_{k=1}^K p_k q_t^k.$$

Define $\zeta^k = (x^k, U^k, V^k)^\top$, with

$$\mathbb{P}(U^k = 1) = r_k, \quad \mathbb{P}(U^k = 0) = 1 - r_k, \qquad \mathbb{P}(V^k = 1) = \mathbb{P}(V^k = 0) = 1/2.$$

For $k = 1, \ldots, K$, let U_t^k and V_t^k be i.i.d. copies of U^k and V^k, respectively. Denote $\zeta_t^k = (x_t^k, U_t^k, V_t^k)^\top$. Define

$$\begin{aligned}
G_k(q_{t-1}^k, \zeta_t^k) = {}& \frac{1 + r_k - 2r_k\tau}{2r_k}\Big[\mathbf{1}\{x_t^k \le q_{t-1}^k\}U_t^k + (1 - U_t^k)(1 - V_t^k)\Big] \\
& - \frac{1 - r_k + 2r_k\tau}{2r_k}\Big[\mathbf{1}\{x_t^k > q_{t-1}^k\}U_t^k + (1 - U_t^k)V_t^k\Big].
\end{aligned} \tag{B.1}$$

Elementary calculations show that

$$g_k(q) := \mathbb{E}G_k(q, \zeta_t^k) = F_k(q) - \tau.$$

Define

$$g(q) = \sum_{k=1}^K p_k g_k(q).$$

Denote

$$\varepsilon_k(q) = G_k(q, \zeta_t^k) - g_k(q).$$

Besides,

$$\mathbb{E}\left(\varepsilon_k^2(q_{t-1}^k)|\mathcal{F}_{t-1}\right) = \frac{1 - r_k^2\{2F_k(q_{t-1}^k) - 1\}^2}{4r_k^2}.$$

By definition, for $t_m \le t < t_{m+1} - 1$, we have

$$q_{t+1}^k = \bar{q}_{t_m} - \eta_m \sum_{i=t_m}^t G_k(q_i^k, \zeta_i^k).$$

Define $s_m = \bar{q}_{t_m} - Q^\star$, and recall that $E_m = t_{m+1} - t_m$ and $\gamma_m = \eta_m E_m$. Elementary Iteration from $t = t_m$ to $t_{m+1} - 1$ yields

$$s_{m+1} = s_m - \eta_m \sum_{t=t_m}^{t_{m+1}-1} \sum_{k=1}^K p_k G_k(q_{t-1}^k, \zeta_t^k) = s_m - \gamma_m \nu_m,$$

in which

$$\nu_m = \frac{1}{E_m} \sum_{t=t_m}^{t_{m+1}-1} \sum_{k=1}^K p_k G_k(q_{t-1}^k, \zeta_t^k).$$

We define
$$h_m := \frac{1}{E_m} \sum_{t=t_m}^{t_{m+1}-1} \sum_{k=1}^{K} p_k G_k \left(\bar{q}_{t_m}; \zeta_t^k \right),$$
and further decompose that
$$\nu_m = G s_m + (g(\bar{q}_{t_m}) - G s_m) + (h_m - g(\bar{q}_{t_m})) + (\nu_m - h_m)$$
$$:= G s_m + r_m + \varepsilon_m + \delta_m,$$
where $G = \sum_{k=1}^{K} p_k f_k(Q^\star)$ is the Hessian at $Q^\star$. It then follows that
$$s_{m+1} = (1 - \gamma_m G) s_m - \gamma_m (r_m + \varepsilon_m + \delta_m) := B_m s_m - \gamma_m U_m, \tag{B.2}$$
where $B_m := 1 - \gamma_m G$ and $U_m := r_m + \varepsilon_m + \delta_m$ for short. Recurring (B.2) gives
$$s_{m+1} = \left(\prod_{j=0}^{m} B_j \right) s_0 - \sum_{j=0}^{m} \left(\prod_{i=j+1}^{m} B_i \right) \gamma_j U_j.$$

Here, we use the convention that $\prod_{i=m+1}^{m} B_i = 1$ for any $m \geq 0$. Recall the definition that
$$h(r, T) = \max \left\{ n \in \mathbb{Z}_+ \,\middle|\, r \sum_{m=1}^{T} \frac{1}{E_m} \geq \sum_{m=1}^{n} \frac{1}{E_m} \right\}.$$

Hence,
$$\frac{\sqrt{t_T}}{T} \sum_{m=0}^{h(r,T)} s_{m+1} = \frac{\sqrt{t_T}}{T} \sum_{m=0}^{h(r,T)} \left[\left(\prod_{j=0}^{m} B_j \right) s_0 - \sum_{j=0}^{m} \left(\prod_{i=j+1}^{m} B_i \right) \gamma_j U_j \right]$$
$$= \frac{\sqrt{t_T}}{T} \sum_{m=0}^{h(r,T)} \left(\prod_{j=0}^{m} B_j \right) s_0 - \frac{\sqrt{t_T}}{T} \sum_{j=0}^{h(r,T)} \sum_{m=j}^{h(r,T)} \left(\prod_{i=j+1}^{m} B_i \right) \gamma_j U_j.$$

For any $n \geq j$, define A_j^n as
$$A_j^n = \sum_{l=j}^{n} \left(\prod_{i=j+1}^{l} B_i \right) \gamma_j.$$

With the notation of A_j^n, we can rewrite that
$$\frac{\sqrt{t_T}}{T} \sum_{m=0}^{h(r,T)} s_{m+1} = \frac{\sqrt{t_T}}{T \gamma_0} A_0^{h(r,T)} B_0 s_0 - \frac{\sqrt{t_T}}{T} \sum_{m=0}^{h(r,T)} A_m^{h(r,T)} U_m.$$

Since $U_m = r_m + \varepsilon_m + \delta_m$, then
$$\frac{\sqrt{t_T}}{T} \sum_{m=0}^{h(r,T)} s_{m+1} + \frac{\sqrt{t_T}}{T} \sum_{m=0}^{h(r,T)} G^{-1} \varepsilon_m = \frac{\sqrt{t_T}}{T \gamma_0} A_0^{h(r,T)} B_0 s_0 - \frac{\sqrt{t_T}}{T} \sum_{m=0}^{h(r,T)} A_m^{h(r,T)} (r_m + \delta_m)$$
$$- \frac{\sqrt{t_T}}{T} \sum_{m=0}^{h(r,T)} \left(A_m^T - G^{-1} \right) \varepsilon_m$$
$$- \frac{\sqrt{t_T}}{T} \sum_{m=0}^{h(r,T)} \left(A_m^{h(r,T)} - A_m^T \right) \varepsilon_m$$
$$=: \mathcal{T}_0 - \mathcal{T}_1 - \mathcal{T}_2 - \mathcal{T}_3.$$

To complete the proof, we first investigate the partial-sum asymptotic behavior of
$$\frac{\sqrt{t_T}}{T} \sum_{m=0}^{h(r,T)} G^{-1} \varepsilon_m,$$

and then show that the four separate terms: $\sup_{r \in [0,1]} \|\mathcal{T}_0\|$, $\sup_{r \in [0,1]} \|\mathcal{T}_1\|$, $\sup_{r \in [0,1]} \|\mathcal{T}_2\|$, and $\sup_{r \in [0,1]} \|\mathcal{T}_4\|$ are $o_{\mathbb{P}}(1)$, respectively.

We aim to follow the proof of Theorem 4.2 in Li et al. (2022). However, we find that the average smoothness condition in their Assumption 3.1 is not satisfied. Due to the presence of the indicator function in (B.1), we only have

$$\sqrt{\mathbb{E}\left\{G_k(x, \zeta_t^k) - G_k(y, \zeta_t^k)\right\}^2} \lesssim |x - y|^{1/2}. \tag{B.3}$$

Upon close examination of their proof, we find that this condition is crucial in the proof of their key Lemma B.2.

In the following, we re-establish the proof of

$$\mathbb{E}|\bar{q}_{t_m} - Q^\star|^2 \lesssim \gamma_m, \quad \bar{q}_{t_m} \xrightarrow{a.s.} Q^*.$$

under the condition given in (B.3). Consider that

$$\mathbb{E}\left(\left|q_{t+1}^k - \bar{q}_{t_m}\right| \big| \mathcal{F}_{t_m}\right) = \eta_m \mathbb{E}\left(\left|\sum_{i=t_m}^{t} G_k(q_i^k, \zeta_i^k)\right| \big| \mathcal{F}_{t_m}\right)$$

$$\leq \eta_m \sum_{i=t_m}^{t} \mathbb{E}\left(|G_k(q_i^k, \zeta_i^k)| | \mathcal{F}_{t_m}\right)$$

$$\lesssim \eta_m \sum_{i=t_m}^{t} \left(1 + |q_i^k - \bar{q}_{t_m}| + |\bar{q}_{t_m} - Q^\star|\right),$$

where the last inequality holds by the following fact

$$\mathbb{E}\left(G_k^2(q_i^k, \zeta_i^k)|\mathcal{F}_i\right) = \mathbb{E}\left(\left|G_k(q_i^k, \zeta_i^k) - g_k(q_i^k)\right|^2 |\mathcal{F}_i\right) + g_k^2(q_i^k)$$

$$\leq \mathbb{E}\left(\left|G_k(q_i^k, \zeta_i^k) - g_k(q_i^k)\right|^2 |\mathcal{F}_i\right) + 2|g_k(q_i^k) - g_k(Q^\star)|^2 + 2g_k^2(Q^\star)$$

$$\lesssim \{1 + 2g_k^2(Q^\star)\} + |q_i^k - Q^\star|^2$$

$$\lesssim 1 + |q_i^k - \bar{q}_{t_m}|^2 + |\bar{q}_{t_m} - Q^\star|^2.$$

Define

$$V_t = \sum_{k=1}^{K} p_k \mathbb{E}\left(|q_t^k - \bar{q}_{t_m}| | \mathcal{F}_{t_m}\right).$$

Hence,

$$V_{t+1} \lesssim \eta_m \sum_{i=t_m}^{t} \left(1 + |\bar{q}_{t_m} - Q^\star| + V_i\right),$$

which further implies that (since $V_{t_m} = 0$)

$$\frac{1}{E_m} \sum_{t=t_m}^{t_{m+1}-1} V_t = \frac{1}{E_m} \sum_{t=t_m}^{t_{m+1}-2} V_{t+1} \lesssim \frac{\eta_m}{E_m} \sum_{t=t_m}^{t_{m+1}-2} \sum_{i=t_m}^{t} \left(1 + |\bar{q}_{t_m} - Q^\star| + V_i\right)$$

$$= \frac{\eta_m}{E_m} \sum_{t=t_m}^{t_{m+1}-2} (t_{m+1} - t - 1)\left(1 + |\bar{q}_{t_m} - Q^\star| + V_t\right)$$

$$\lesssim \eta_m \sum_{t=t_m}^{t_{m+1}-2} \left(1 + |\bar{q}_{t_m} - Q^\star| + V_t\right)$$

$$\lesssim \eta_m E_m \left(1 + |\bar{q}_{t_m} - Q^\star| + \frac{1}{E_m} \sum_{t=t_m}^{t_{m+1}-1} V_t\right).$$

Denote by $\gamma_m = \eta_m E_m$. It follows that

$$\frac{1}{E_m} \sum_{t=t_m}^{t_{m+1}-1} V_t \lesssim \gamma_m \left(1 + |\bar{q}_{t_m} - Q^\star|\right). \tag{B.4}$$

Let $\mathcal{G}_k(\cdot)$ denote an antiderivative of $g_k(\cdot)$, and $\mathcal{G}(\cdot) = \sum_{k=1}^K p_k \mathcal{G}_k(\cdot)$. Let $\Delta_m = \mathcal{G}(\bar{q}_{t_m}) - \mathcal{G}(Q^\star)$. The equation (17) in Li et al. (2022) shows that for some constant $L > 0$,

$$\mathbb{E}\left\{\mathcal{G}(\bar{q}_{t_{m+1}}) | \mathcal{F}_{t_m}\right\} \leq \mathcal{G}(\bar{q}_{t_m}) - \gamma_m/2 \left|\nabla\mathcal{G}(\bar{q}_{t_m})\right|^2 + \gamma_m^2 L \mathbb{E}(h_m^2 | \mathcal{F}_{t_m}) + \left(\gamma_m/2 + \gamma_m^2 L\right) \mathbb{E}(\delta_m^2 | \mathcal{F}_{t_m}),$$

where

$$h_m = \frac{1}{E_m} \sum_{t=t_m}^{t_{m+1}-1} \sum_{k=1}^K p_k \nabla G_k(\bar{q}_{t_m}^k, \zeta_t^k), \quad \delta_m = \frac{1}{E_m} \sum_{t=t_m}^{t_{m+1}-1} \sum_{k=1}^K p_k \nabla G_k(\bar{q}_t^k, \zeta_t^k).$$

Lemma B.9 of Li et al. (2022) obtains that

$$\mathbb{E}(h_m^2 | \mathcal{F}_{t_m}) \leq |\nabla\mathcal{G}(\bar{q}_{t_m})|^2 + \frac{C_1}{E_m} + \frac{C_2}{E_m}|\bar{q}_{t_m} - Q^\star|^2.$$

Notice that

$$\mathbb{E}\left\{\left(G_k(q_{t-1}^k, \zeta_t^k) - G_k(\bar{q}_{t_m}, \zeta_t^k)\right)^2 | \mathcal{F}_{t_m}\right\} \lesssim \mathbb{E}\left(|q_t^k - \bar{q}_{t_m}| \, | \mathcal{F}_{t_m}\right).$$

Thus,

$$\mathbb{E}(\delta_m^2 | \mathcal{F}_{t_m}) \lesssim \frac{1}{E_m} \sum_{t=t_m}^{t_{m+1}-1} \sum_{k=1}^K p_k \mathbb{E}\left\{\left(G_k(q_{t-1}^k, \zeta_t^k) - G_k(\bar{q}_{t_m}, \zeta_t^k)\right)^2 | \mathcal{F}_{t_m}\right\}$$

$$\lesssim \frac{1}{E_m} \sum_{t=t_m}^{t_{m+1}-1} \sum_{k=1}^K p_k \mathbb{E}\left(|q_t^k - \bar{q}_{t_m}| \, | \mathcal{F}_{t_m}\right)$$

$$\lesssim \gamma_m \left(1 + |\bar{q}_{t_m} - Q^\star|\right),$$

where the last inequality holds by (B.4). Therefore, we obtain that

$$\mathbb{E}(\Delta_{m+1} | \mathcal{F}_{t_m}) \leq \Delta_m - \gamma_m/2 |\nabla\mathcal{G}(\bar{q}_{t_m})|^2 + \gamma_m^2 L \left\{|\nabla\mathcal{G}(\bar{q}_{t_m})|^2 + \frac{C_1}{E_m} + \frac{C_2}{E_m}|\bar{q}_{t_m} - Q^\star|^2\right\}$$

$$+ \left(\gamma_m/2 + \gamma_m^2 L\right) \gamma_m \left(C_1 + C_2 |\bar{q}_{t_m} - Q^*|\right)$$

$$\leq (1 - c_1\gamma_m + c_2\gamma_m^2)\Delta_m + \left(c_3 + c_4\Delta_m^{1/2}\right)\gamma_m^2.$$

Since we assume that the parameter space is uniformly bounded, it entails that Δ_m is also uniformly bounded. Thus, we have

$$\mathbb{E}(\Delta_{m+1} | \mathcal{F}_{t_m}) \leq (1 - c_1\gamma_m + c_2\gamma_m^2)\Delta_m + (c_3 + c_5)\gamma_m^2.$$

Apply Robbins-Siegmund theorem in Robbins & Siegmund (1971) to obtain $\bar{q}_{t_m} \to Q^\star$ almost surely. Lemma A.10 in Su & Zhu (2018) states that for any positive constants c_1, c_2, if $\gamma_m = o(1)$, $\gamma_{m-1}/\gamma_m = 1 + o(\gamma_m)$, and B_m is a positive sequence, satisfying

$$B_m \leq \frac{\gamma_{m-1}(1 - c_1\gamma_m)}{\gamma_m} B_{m-1} + c_2\gamma_m,$$

then $\sup_m B_m < \infty$. Using this lemma, we immediately obtain that for some positive constant $C > 0$,

$$\sup_{m \geq 1} \frac{\mathbb{E}\Delta_m}{\gamma_{m-1}} < C,$$

which entails that

$$\mathbb{E}|\bar{q}_{t_m} - Q^\star|^2 \lesssim \mathbb{E}\Delta_m \lesssim \gamma_{m-1} \lesssim \gamma_m \{1 + o(\gamma_m)\} \lesssim \gamma_m.$$

To demonstrate that our setting satisfies Assumption 3.2 of Li et al. (2022), we define

$$S_k := \mathbb{E}\varepsilon_k^2(Q^\star) = \frac{1 - r_k^2 \{2F_k(Q^\star) - 1\}^2}{4r_k^2} = \frac{1 - r_k^2 \{2Q_k - 1\}^2}{4r_k^2}.$$

Hence,

$$\left| \mathbb{E}\left(\varepsilon_k^2(q_{t-1}^k)|\mathcal{F}_{t-1}\right) - \mathbb{E}\varepsilon_k^2(Q^\star) \right| \lesssim |q_{t-1}^k - Q^\star|,$$

satisfying Assumption 3.2 in Li et al. (2022). Assumptions 3.3 and 3.4 of Li et al. (2022) are the same as our Assumptions 3-4.

By closely examining the proof of Li et al. (2022), we find that their Assumption 3.1 is used exclusively to establish the $\mathcal{L}^2$ convergence rate and the almost sure convergence result in their Lemma B.2. The appearance of Assumption 1 in the conditions of their Lemma B.3, which derivs the functional weak convergence, is solely for enabling the application of Lemma B.2.

In our analysis, however, the key bound $\mathbb{E}|\bar{q}_{t_m} - Q^\star|^2 \lesssim \gamma_m$ is proved directly under equation (B.3). This bound fully replaces the role played by Lemma B.2 in Li et al. (2022). Consequently, Assumption 3.1 of Li et al. (2022) is not needed in our theoretical development beyond this step, and the functional central limit theorem follows without invoking that assumption.

Recall that

$$\varepsilon_m = \frac{1}{E_m} \sum_{t=t_m}^{t_{m+1}-1} \sum_{k=1}^{K} p_k \left\{ G_k(\bar{q}_{t_m}, \zeta_t^k) - g(\bar{q}_{t_m}) \right\}.$$

Define $U_T^2 = \sum_{m=1}^{T} \mathbb{E}(\varepsilon_m^2|\mathcal{F}_{t_m})$ and

$$\Xi_T(r) := U_T^{-1} \left\{ \sum_{m=1}^{i} \varepsilon_m + \frac{(rU_T^2 - U_i^2)\varepsilon_{i+1}}{U_{i+1}^2 - U_i^2} \right\} \quad U_i^2 \le rU_T^2 < U_{i+1}^2.$$

Then,

$$\frac{\sqrt{t_T}}{T} \sum_{m=1}^{h(r,T)} \varepsilon_m = \frac{\sqrt{t_T}}{T} U_T \Xi_T \left(\frac{U_{h(r,T)}^2}{U_T^2} \right).$$

Following Lemma B.16 in Li et al. (2022), one obtains that

$$\sup_{r \in [0,1]} \left| \frac{\sqrt{t_T}}{T} U_T \Xi_T \left(\frac{U_{h(r,T)}^2}{U_T^2} \right) - \frac{\sqrt{t_T}}{T} U_T \Xi_T(r) \right| \xrightarrow{\mathbb{P}} 0. \tag{B.5}$$

By evaluating the conditions in Lemma B.13 of Li et al. (2022), the invariance principles in the martingale CLT yileds that $\Xi_T(r) \xrightarrow{d} B(r)$ in $\mathcal{C}[0,1]$, which is followed by

$$\frac{\sqrt{t_T}}{T} U_T \Xi_T(r) \xrightarrow{d} \frac{\sqrt{\nu \sum_{k=1}^{K} p_k^2 \{r_k^{-2} - (2Q_k - 1)^2\}}}{2 \sum_{k=1}^{K} p_k f_k(Q^\star)} B(r).$$

Hus, Theorem A.2 of Hall & Heyde (2014) implies that $\left\{ \sqrt{t_T} U_T \Xi_T(\cdot)/T \right\}_{T \ge 1}$ is tight in $\mathcal{C}[0,1]$. Using the tightness of $\left\{ \sqrt{t_T} U_T \Xi_T(\cdot)/T \right\}_{T \ge 1}$ and (B.5), we could obtain the tightness

$$\left\{ \frac{\sqrt{t_T}}{T} U_T \Xi_T \left(\frac{U_{h(r,T)}^2}{U_T^2} \right) \right\}_{T \ge 1}$$

following the arguments in the proof of Lemma B.16 of Li et al. (2022). Therefore, we could follow the arguments in the proof of Theorem 4.2 in Li et al. (2022) to complete the proof the functional CLT.

C ADDITIONAL EXPERIMENTS AND DISCUSSIONS

In this section, we report additional simulation results that complement the main experiments in Section 4. Unless otherwise specified, all settings are identical to those in Section 4.1.
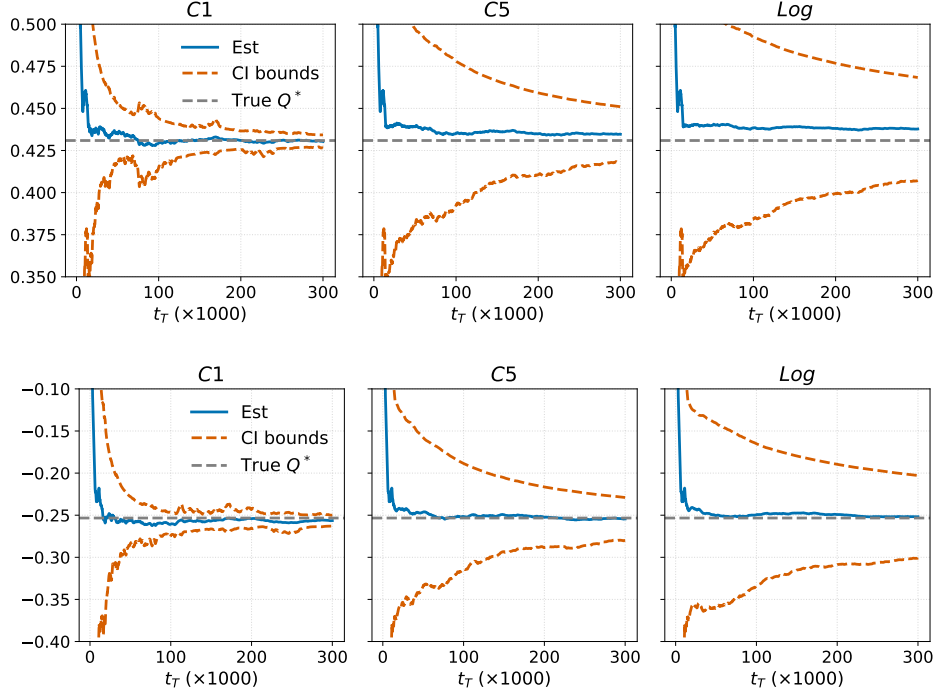
Figure S.1: Sample trajectories of the iterative estimator and corresponding confidence intervals under heterogeneous distributions (Hete L, with $r_k = 0.9$ and $\tau = 0.5$, upper panel) and heterogeneous quantile levels (τ_{low}, with heterogeneous response rates, lower panel). The horizontal dotted line indicates the true quantile value Q^*.

Quantile (τ)	Rate (r)	C1	C5	Log	DP-SGD (C1)	DC	Single
				$t_T = 10000$			
0.5	0.25	0.950(0.0160)	0.979(0.0250)	0.978(0.0324)	0.952(0.0242)	0.802(0.3197)	0.926(0.0179)
0.5	hetero	0.953(0.0086)	0.994(0.0124)	0.993(0.0168)	0.956(0.0125)	0.999(0.0678)	0.942(0.0075)
0.5	0.9	1.000(0.0027)	1.000(0.0057)	1.000(0.0097)	0.987(0.0044)	1.000(0.0216)	0.954(0.0047)
τ_{low}	0.25	0.929(0.0196)	0.976(0.0270)	0.978(0.0349)	0.911(0.0309)	0.740(0.3403)	0.930(0.0194)
τ_{low}	hetero	0.923(0.0118)	0.983(0.0131)	0.983(0.0174)	0.896(0.0181)	0.999(0.0735)	0.960(0.0083)
τ_{low}	0.9	0.969(0.0055)	0.999(0.0047)	1.000(0.0081)	0.922(0.0074)	1.000(0.0231)	0.954(0.0054)
τ_{high}	0.25	0.956(0.0205)	0.972(0.0310)	0.971(0.0399)	0.944(0.0313)	0.729(0.3768)	0.944(0.0213)
τ_{high}	hetero	0.956(0.0109)	0.986(0.0145)	0.988(0.0198)	0.959(0.0160)	0.997(0.0839)	0.954(0.0089)
τ_{high}	0.9	0.999(0.0049)	0.997(0.0046)	1.000(0.0068)	0.989(0.0059)	1.000(0.0259)	0.974(0.0059)
				$t_T = 50000$			
0.5	0.25	0.960(0.0070)	0.987(0.0101)	0.991(0.0144)	0.955(0.0104)	0.977(0.0787)	0.958(0.0071)
0.5	hetero	0.975(0.0037)	0.986(0.0052)	0.994(0.0077)	0.975(0.0055)	1.000(0.0156)	0.970(0.0030)
0.5	0.9	1.000(0.0010)	1.000(0.0016)	1.000(0.0029)	0.995(0.0019)	1.000(0.0051)	0.950(0.0020)
τ_{low}	0.25	0.913(0.0104)	0.973(0.0119)	0.988(0.0154)	0.878(0.0171)	0.973(0.0863)	0.946(0.0079)
τ_{low}	hetero	0.819(0.0076)	0.942(0.0070)	0.977(0.0084)	0.786(0.0116)	0.999(0.0166)	0.952(0.0034)
τ_{low}	0.9	0.987(0.0042)	0.988(0.0018)	0.999(0.0022)	0.854(0.0054)	1.000(0.0054)	0.962(0.0021)
τ_{high}	0.25	0.951(0.0107)	0.986(0.0163)	0.980(0.0250)	0.910(0.0183)	0.976(0.0983)	0.950(0.0089)
τ_{high}	hetero	0.967(0.0057)	0.995(0.0103)	0.988(0.0164)	0.924(0.0110)	1.000(0.0189)	0.946(0.0039)
τ_{high}	0.9	1.000(0.0012)	1.000(0.0043)	1.000(0.0083)	0.995(0.0027)	1.000(0.0059)	0.946(0.0024)

Table S.2: Empirical coverage probabilities at the 95% nominal level (mean absolute errors ↓) under varying quantile levels and response rates, with different t_T and fixed $K = 10$ clients and data generated from $\mathcal{C}(0, 1)$. In Case τ_{low}, each client uses a unique quantile level τ_k ranging uniformly from $[0.3, 0.5]$; in Case τ_{high}, τ_k is ranging from $[0.5, 0.8]$. "hetero" indicates client-specific truthful response rates r_k range uniformly from $[0.25, 0.9]$.

Quantile (τ)	Rate (r)	C1	C5	Log	DP-SGD (C1)	DC	Single
				$t_T = 10000$			
0.3	0.25	0.947(0.0271)	0.981(0.0400)	0.967(0.0545)	0.925(0.0423)	0.546(0.6111)	0.946(0.0339)
0.3	hetero	0.957(0.0138)	0.994(0.0231)	0.992(0.0311)	0.942(0.0223)	0.682(0.3476)	0.948(0.0137)
0.3	0.9	1.000(0.0039)	1.000(0.0170)	1.000(0.0254)	0.994(0.0066)	0.070(0.3084)	0.972(0.0083)
0.5	0.25	0.942(0.0225)	0.983(0.0298)	0.977(0.0389)	0.935(0.0314)	0.968(0.3335)	0.936(0.0264)
0.5	hetero	0.946(0.0132)	0.970(0.0155)	0.981(0.0196)	0.951(0.0170)	1.000(0.0757)	0.942(0.0109)
0.5	0.9	0.976(0.0095)	0.994(0.0053)	0.998(0.0064)	0.953(0.0100)	0.968(0.0519)	0.968(0.0071)
0.8	0.25	0.935(0.0450)	0.958(0.0729)	0.960(0.0963)	0.938(0.0677)	0.087(1.0105)	0.950(0.0552)
0.8	hetero	0.956(0.0232)	0.963(0.0370)	0.971(0.0457)	0.963(0.0343)	0.557(0.5459)	0.968(0.0210)
0.8	0.9	0.985(0.0171)	0.836(0.0269)	0.933(0.0267)	0.971(0.0165)	0.161(0.4245)	0.982(0.0122)
				$t_T = 50000$			
0.3	0.25	0.902(0.0151)	0.979(0.0165)	0.988(0.0225)	0.863(0.0253)	0.798(0.3556)	0.958(0.0137)
0.3	hetero	0.835(0.0102)	0.975(0.0081)	0.994(0.0108)	0.831(0.0164)	0.023(0.3026)	0.948(0.0059)
0.3	0.9	0.984(0.0056)	1.000(0.0034)	1.000(0.0079)	0.869(0.0072)	0.000(0.2951)	0.938(0.0037)
0.5	0.25	0.935(0.0100)	0.983(0.0127)	0.986(0.0180)	0.926(0.0144)	1.000(0.0910)	0.958(0.0108)
0.5	hetero	0.942(0.0063)	0.981(0.0064)	0.995(0.0093)	0.947(0.0081)	0.853(0.0496)	0.954(0.0045)
0.5	0.9	0.998(0.0049)	0.999(0.0017)	1.000(0.0039)	0.959(0.0052)	0.477(0.0481)	0.948(0.0029)
0.8	0.25	0.926(0.0247)	0.991(0.0344)	0.986(0.0514)	0.887(0.0437)	0.522(0.5824)	0.952(0.0202)
0.8	hetero	0.925(0.0149)	0.990(0.0231)	0.990(0.0371)	0.890(0.0278)	0.079(0.4077)	0.950(0.0086)
0.8	0.9	1.000(0.0038)	1.000(0.0107)	1.000(0.0197)	0.979(0.0077)	0.001(0.3822)	0.968(0.0049)

Table S.3: Empirical coverage probabilities at the 95% nominal level (mean absolute errors ↓) under heterogeneous distributions for different t_T. The number of clients K is fixed at 10. Data for each client k are independently generated from $\mathcal{C}(\mu_k, 1)$, where $\mu_k \sim \mathcal{N}(0, 1)$. "hetero" indicates client-specific truthful response rates r_k range uniformly from $[0.25, 0.9]$.

Quantile (τ)	Rate (r)	C1	C5	Log
		$T = 5000$		
0.5	0.25	0.954(0.0189)	0.974(0.0129)	0.986(0.0112)
0.5	hetero	0.959(0.0103)	0.976(0.0065)	0.995(0.0052)
0.5	0.9	0.999(0.0033)	1.000(0.0040)	1.000(0.0026)
τ_{low}	0.25	0.957(0.0200)	0.974(0.0137)	0.991(0.0116)
τ_{low}	hetero	0.957(0.0108)	0.977(0.0067)	0.993(0.0053)
τ_{low}	0.9	1.000(0.0033)	1.000(0.0040)	1.000(0.0029)
τ_{high}	0.25	0.956(0.0212)	0.975(0.0128)	0.993(0.0123)
τ_{high}	hetero	0.961(0.0112)	0.984(0.0062)	0.996(0.0056)
τ_{high}	0.9	0.998(0.0037)	0.997(0.0028)	1.000(0.0031)
		$T = 10000$		
0.5	0.25	0.949(0.0133)	0.968(0.0078)	0.987(0.0061)
0.5	hetero	0.963(0.0071)	0.978(0.0037)	0.991(0.0030)
0.5	0.9	0.995(0.0023)	0.999(0.0020)	0.999(0.0014)
τ_{low}	0.25	0.947(0.0136)	0.972(0.0078)	0.984(0.0064)
τ_{low}	hetero	0.962(0.0072)	0.985(0.0038)	0.983(0.0033)
τ_{low}	0.9	0.999(0.0020)	1.000(0.0016)	0.967(0.0018)
τ_{high}	0.25	0.939(0.0145)	0.974(0.0086)	0.985(0.0066)
τ_{high}	hetero	0.968(0.0076)	0.988(0.0043)	0.985(0.0032)
τ_{high}	0.9	0.996(0.0023)	0.999(0.0031)	0.996(0.0014)

Table S.4: Empirical coverage probabilities at the 95% nominal level (mean absolute errors ↓) under varying quantile levels and response rates, with different T and fixed $K = 10$ clients and data generated from $\mathcal{N}(0, 1)$. In Case τ_{low}, each client uses a unique quantile level τ_k ranging uniformly from $[0.3, 0.5]$; in Case τ_{high}, τ_k is ranging from $[0.5, 0.8]$. "hetero" indicates client-specific truthful response rates r_k range uniformly from $[0.25, 0.9]$.

Quantile (τ)	Rate (r)	C1	C5	Log
		Hete L — $T = 5000$		
0.3	0.25	0.942(0.0271)	0.960(0.0168)	0.975(0.0151)
0.3	hetero	0.962(0.0131)	0.966(0.0086)	0.987(0.0067)
0.3	0.9	0.998(0.0043)	0.959(0.0063)	1.000(0.0033)
0.5	0.25	0.954(0.0254)	0.973(0.0154)	0.990(0.0153)
0.5	hetero	0.963(0.0120)	0.981(0.0072)	0.991(0.0071)
0.5	0.9	0.992(0.0042)	0.998(0.0032)	1.000(0.0034)
0.8	0.25	0.954(0.0375)	0.982(0.0242)	0.998(0.0248)
0.8	hetero	0.968(0.0181)	0.988(0.0109)	0.998(0.0116)
0.8	0.9	0.985(0.0108)	0.999(0.0070)	0.982(0.0094)
		Hete L — $T = 10000$		
0.3	0.25	0.958(0.0184)	0.966(0.0102)	0.981(0.0083)
0.3	hetero	0.949(0.0096)	0.965(0.0050)	0.979(0.0040)
0.3	0.9	1.000(0.0029)	0.979(0.0022)	0.867(0.0036)
0.5	0.25	0.950(0.0165)	0.974(0.0094)	0.985(0.0085)
0.5	hetero	0.952(0.0085)	0.976(0.0045)	0.991(0.0039)
0.5	0.9	0.996(0.0025)	0.985(0.0018)	1.000(0.0016)
0.8	0.25	0.966(0.0237)	0.983(0.0163)	0.990(0.0149)
0.8	hetero	0.962(0.0122)	0.988(0.0088)	0.974(0.0090)
0.8	0.9	0.990(0.0042)	0.997(0.0087)	0.645(0.0095)
		Hete D — $T = 5000$		
0.5	0.25	0.954(0.0195)	0.974(0.0129)	0.987(0.0109)
0.5	hetero	0.965(0.0098)	0.974(0.0075)	0.993(0.0049)
0.5	0.9	1.000(0.0037)	0.989(0.0060)	1.000(0.0026)
		Hete D — $T = 10000$		
0.5	0.25	0.949(0.0132)	0.968(0.0078)	0.982(0.0064)
0.5	hetero	0.966(0.0069)	0.973(0.0039)	0.972(0.0034)
0.5	0.9	1.000(0.0023)	0.999(0.0014)	0.966(0.0023)

Table S.5: Empirical coverage probabilities at the 95% nominal level (mean absolute errors ↓) under heterogeneous distributions for different T. The number of clients K is fixed at 10. In Hete L, data for each client k are independently generated from $\mathcal{N}(\mu_k, 1)$, where $\mu_k \sim \mathcal{N}(0, 1)$. In Hete D, data are generated from $\mathcal{N}(0, 1)$, $\mathcal{U}(-1, 1)$, and $\mathcal{C}(0, 1)$ across different clients. "hetero" indicates client-specific truthful response rates r_k range uniformly from $[0.25, 0.9]$.

C.1   OTHER RESULTS IN SECTION 4

Efficiency–Accuracy Trade-off.   We first quantitatively study the computation and communication time of the proposed method. Specifically, for each simulation run, we record the wall-clock time, including both computation and communication components, and then average the results over 1,000 repetitions. We consider different communication strategies for the proposed estimators as well as the competing baselines. Figure S.2 reports the results for a representative setting with quantile level $\tau_k \equiv \tau = 0.5$, truthful response rate $r_k \equiv r = 0.5$, data generated from a standard normal distribution, and total sample size $t_T = 10,000$. We obtain the following interesting findings. First, for the proposed methods, as the communication frequency increases, the MAE decreases, but both computation time and communication cost naturally grow, demonstrating a clear efficiency–accuracy trade-off. In addition, comparing across different methods, the proposed method attains a communication cost comparable to DP-SGD while requiring noticeably less computation time. The DC method incurs the lowest overall cost because it performs only a single aggregation step; however, it also exhibits the largest MAE and substantial under-coverage in several heterogeneous settings, as reported in Section 4.

Partial Participation.   We further examine partial client participation to evaluate the proposed method in more realistic federated environments. In this setting, at each communication round, only 5 out of the 10 clients are randomly selected to participate, while all other configurations remain identical to those in Section 4.1. The results are reported in Tables S.6 and S.7. We observe that
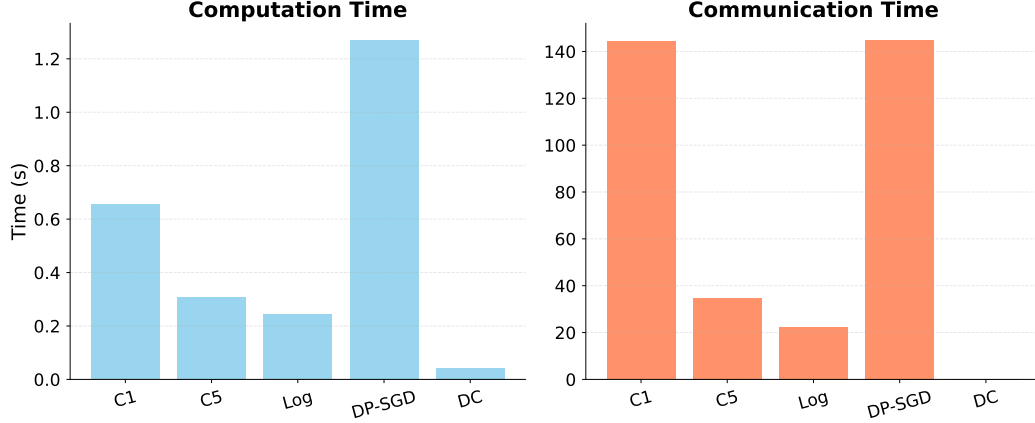
Figure S.2: Computation time and communication time for different methods. We fix $K = 10$ and $t_T = 10{,}000$.

the empirical coverage probabilities remain close to the nominal 95% level, and the MAE increases only mildly compared with the full-participation case. These findings indicate that the proposed estimator is robust to partial and asynchronous client participation.

C.2 SENSITIVITY ANALYSIS

We begin by examining how the proposed method responds to different truthful response rates r and step-size schedules. Throughout this subsection, we adopt the normal design with $X \sim \mathcal{N}(0,1)$ and target quantile level $\tau_k \equiv \tau = 0.5$, and we consider $E'_m = 5$ and $t_T \in \{10{,}000, 50{,}000\}$. All other settings follow Section 4.1.

First, we conduct a sensitivity analysis on the truthful response rate. The results are reported in Figure S.3. We observe that both the MAE and the average interval length steadily decrease as r increases, while the ECP remains close to or above the nominal 95% level across a wide range of response rates.

Second, we investigate the effect of the step-size schedule. We adopt

$$\gamma_m = \frac{20\,\bar{r}}{m^a + 100},$$

where $\bar{r}$ denotes the average truthful response rate and $a > 0$ controls the decay speed. Figure S.4 summarizes the results. Under the same experimental setting, the MAE, ECP, and Avg Len (average confidence-interval lengths) remain comparable across different values of a. This indicates that the proposed estimator is stable with respect to the choice of the step-size schedule.

C.3 CONSERVATIVENESS OF THE SELF-NORMALIZED INFERENCE PROCEDURE

To assess the efficiency and conservativeness of the resulting confidence intervals, we compare the resulting confidence intervals with oracle normal-based intervals that use the true asymptotic variance derived in Theorem 3.1. Tables S.8–S.9 report the empirical coverage probabilities (ECP) and average interval lengths (Avg Len) for both types of intervals under normal and Cauchy data-generating distributions. We observe that compared with the oracle intervals, the self-normalized intervals are slightly conservative: they achieve coverage at or above the nominal 95% level but produce moderately wider intervals. This mild conservativeness arises because self-normalization induces heavier-tailed limiting distributions compared with the standard normal approximation. It is important to note, however, that estimating the oracle variance in practice typically requires additional procedures that may consume further privacy budget under LDP. In contrast, the self-normalized construction avoids any variance estimation and remains fully privacy-preserving.

C.4 Extension to Decentralized Federated Learning

In this subsection, we provide an initial exploration of extending our method to a fully decentralized federated learning setting, where no central server is available and each client communicates only with its neighbors. Let the K clients be connected through an undirected communication graph represented by an adjacency matrix $A = (a_{k_1 k_2}) \in \mathbb{R}^{K \times K}$, where $a_{k_1 k_2} = 1$ if client k_1 can exchange messages with client k_2 and $a_{k_1 k_2} = 0$ otherwise. Here we assume that every client is connected to itself, i.e., $a_{kk} = 1$, $k = 1, \ldots, K$. Define the degree $d_{k_1} = \sum_{k_2} a_{k_1 k_2}$ and construct the row-stochastic weight matrix $W = (w_{k_1 k_2})$ as

$$w_{k_1 k_2} = \frac{a_{k_1 k_2}}{d_{k_1}},$$

which encodes the network topology and performs neighbor averaging.

During communication iterations $t \in \mathcal{I}$, the aggregation step in Algorithm 1 is replaced by the following *weighted decentralized averaging*:

$$q_{t_m}^k \leftarrow \sum_{j=1}^{K} w_{kj} \, p_j \, q_{t_m}^j, \qquad k = 1, \ldots, K.$$

The local SGD update for $t \notin \mathcal{I}$ remains unchanged, yielding a fully decentralized variant of our estimator.

As a preliminary empirical study of this extension, we evaluate its finite-sample performance under a ring network topology, where each client communicates only with itself and its two immediate neighbors. All other experimental settings follow Section 4.1. The results in Table S.10 show that the decentralized estimator exhibits qualitatively similar behavior to its federated counterpart, suggesting that our method can naturally extend to decentralized learning. A complete theoretical analysis of this decentralized variant is left for future work.
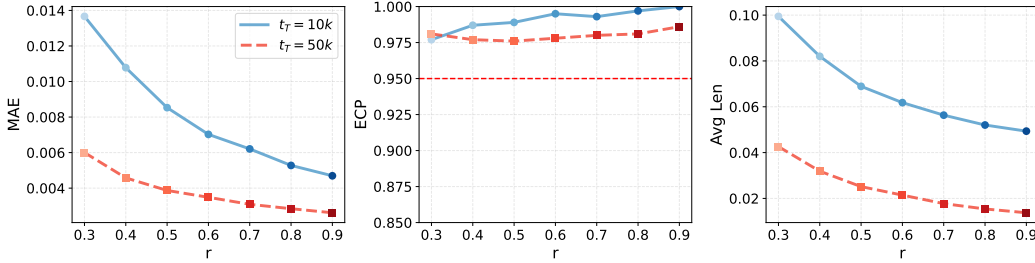

Figure S.3: Mean absolute errors (MAE ↓), empirical coverage probabilities at the 95% nominal level (ECP), and averaged confidence interval lengths (Avg Len ↓) under varying response rates. We fix $\tau_k \equiv \tau = 0.5$ and $K = 10$, and report results for different values of t_T with data generated from $\mathcal{N}(0, 1)$.

Scenario	Quantile (τ)	Rate (r)	C1	C5	Log
			$t_T = 10\,000$		
	0.5	0.25	0.950(0.0186)	0.971(0.0292)	0.979(0.0417)
	0.5	hetero	0.942(0.0102)	0.976(0.0140)	0.993(0.0194)
	0.5	0.9	0.955(0.0047)	0.988(0.0062)	0.998(0.0087)
	τ_{low}	0.25	0.949(0.0190)	0.975(0.0305)	0.984(0.0433)
Homo	τ_{low}	hetero	0.953(0.0097)	0.981(0.0146)	0.994(0.0203)
	τ_{low}	0.9	0.985(0.0032)	0.999(0.0064)	1.000(0.0091)
	τ_{high}	0.25	0.947(0.0208)	0.971(0.0316)	0.982(0.0461)
	τ_{high}	hetero	0.928(0.0126)	0.984(0.0155)	0.993(0.0219)
	τ_{high}	0.9	0.973(0.0058)	0.997(0.0062)	1.000(0.0100)
	0.3	0.25	0.942(0.0255)	0.971(0.0401)	0.972(0.0565)
	0.3	hetero	0.951(0.0127)	0.968(0.0198)	0.983(0.0258)
	0.3	0.9	0.946(0.0054)	0.961(0.0091)	0.990(0.0119)
	0.5	0.25	0.955(0.0225)	0.970(0.0375)	0.984(0.0531)
Hete L	0.5	hetero	0.946(0.0116)	0.981(0.0180)	0.997(0.0247)
	0.5	0.9	0.978(0.0044)	0.993(0.0078)	0.995(0.0119)
	0.8	0.25	0.955(0.0339)	0.975(0.0614)	0.986(0.0890)
	0.8	hetero	0.964(0.0171)	0.987(0.0279)	0.992(0.0387)
	0.8	0.9	0.998(0.0050)	0.988(0.0147)	0.993(0.0197)
			$t_T = 50\,000$		
	0.5	0.25	0.962(0.0081)	0.984(0.0106)	0.998(0.0158)
	0.5	hetero	0.962(0.0040)	0.988(0.0055)	0.996(0.0080)
	0.5	0.9	1.000(0.0012)	1.000(0.0017)	1.000(0.0028)
	τ_{low}	0.25	0.945(0.0090)	0.986(0.0110)	0.994(0.0163)
Homo	τ_{low}	hetero	0.970(0.0047)	0.989(0.0058)	0.995(0.0086)
	τ_{low}	0.9	1.000(0.0020)	1.000(0.0020)	1.000(0.0030)
	τ_{high}	0.25	0.950(0.0088)	0.978(0.0118)	0.998(0.0176)
	τ_{high}	hetero	0.942(0.0044)	0.983(0.0062)	0.997(0.0090)
	τ_{high}	0.9	0.984(0.0017)	0.998(0.0036)	0.999(0.0056)
	0.3	0.25	0.943(0.0123)	0.974(0.0155)	0.990(0.0228)
	0.3	hetero	0.937(0.0067)	0.982(0.0071)	0.994(0.0106)
	0.3	0.9	0.992(0.0022)	0.991(0.0029)	0.997(0.0045)
	0.5	0.25	0.952(0.0099)	0.981(0.0136)	0.994(0.0202)
Hete L	0.5	hetero	0.966(0.0051)	0.974(0.0065)	0.992(0.0093)
	0.5	0.9	0.978(0.0021)	0.974(0.0028)	0.993(0.0040)
	0.8	0.25	0.948(0.0152)	0.984(0.0207)	0.990(0.0300)
	0.8	hetero	0.949(0.0074)	0.962(0.0102)	0.995(0.0139)
	0.8	0.9	0.902(0.0035)	0.954(0.0084)	0.991(0.0097)

Table S.6: Empirical coverage probabilities at the 95% nominal level (mean absolute errors $\downarrow$) under varying quantile levels and truthful response rates, with different values of t_T and a fixed number of $K = 10$ clients. Only 5 out of the 10 clients are randomly selected to participate in each communication round. In Homo, data for each client k are independently drawn from $\mathcal{N}(0, 1)$. In Hete L, client-specific data are independently drawn from $\mathcal{N}(\mu_k, 1)$ with $\mu_k \sim \mathcal{N}(0, 1)$. The label "hetero" indicates heterogeneous truthful response rates with r_k ranging uniformly from 0.25 to 0.9.

Scenario	Quantile (τ)	Rate (r)	C1	C5	Log
			$t_T = 10\,000$		
	0.5	0.25	0.950(0.0232)	0.973(0.0353)	0.968(0.0473)
	0.5	hetero	0.966(0.0114)	0.991(0.0169)	0.991(0.0229)
	0.5	0.9	1.000(0.0034)	1.000(0.0062)	0.999(0.0100)
	τ_{low}	0.25	0.936(0.0279)	0.974(0.0393)	0.967(0.0509)
Homo	τ_{low}	hetero	0.928(0.0150)	0.989(0.0187)	0.988(0.0241)
	τ_{low}	0.9	0.997(0.0048)	1.000(0.0068)	1.000(0.0105)
	τ_{high}	0.25	0.940(0.0333)	0.965(0.0466)	0.961(0.0621)
	τ_{high}	hetero	0.951(0.0184)	0.985(0.0246)	0.980(0.0338)
	τ_{high}	0.9	1.000(0.0045)	1.000(0.0088)	0.999(0.0132)
	0.3	0.25	0.947(0.0396)	0.968(0.0588)	0.952(0.0763)
	0.3	hetero	0.956(0.0199)	0.984(0.0306)	0.993(0.0397)
	0.3	0.9	0.999(0.0069)	0.999(0.0257)	1.000(0.0356)
	0.5	0.25	0.940(0.0309)	0.963(0.0432)	0.968(0.0561)
Hete L	0.5	hetero	0.965(0.0148)	0.989(0.0220)	0.980(0.0284)
	0.5	0.9	0.999(0.0046)	0.998(0.0076)	0.998(0.0112)
	0.8	0.25	0.935(0.0743)	0.956(0.1039)	0.956(0.1376)
	0.8	hetero	0.947(0.0423)	0.975(0.0539)	0.972(0.0687)
	0.8	0.9	0.993(0.0114)	0.996(0.0145)	0.990(0.0192)
			$t_T = 50\,000$		
	0.5	0.25	0.943(0.0106)	0.985(0.0148)	0.984(0.0211)
	0.5	hetero	0.970(0.0053)	0.986(0.0087)	0.989(0.0121)
	0.5	0.9	1.000(0.0023)	1.000(0.0050)	0.997(0.0072)
	τ_{low}	0.25	0.896(0.0147)	0.988(0.0178)	0.986(0.0248)
Homo	τ_{low}	hetero	0.902(0.0087)	0.980(0.0092)	0.991(0.0124)
	τ_{low}	0.9	1.000(0.0028)	1.000(0.0027)	0.999(0.0044)
	τ_{high}	0.25	0.893(0.0205)	0.982(0.0293)	0.971(0.0431)
	τ_{high}	hetero	0.930(0.0130)	0.990(0.0212)	0.985(0.0316)
	τ_{high}	0.9	1.000(0.0046)	1.000(0.0104)	1.000(0.0161)
	0.3	0.25	0.895(0.0232)	0.970(0.0272)	0.989(0.0377)
	0.3	hetero	0.875(0.0138)	0.983(0.0140)	0.987(0.0188)
	0.3	0.9	1.000(0.0046)	1.000(0.0047)	0.990(0.0089)
	0.5	0.25	0.957(0.0136)	0.984(0.0193)	0.985(0.0274)
Hete L	0.5	hetero	0.988(0.0068)	0.991(0.0100)	0.991(0.0154)
	0.5	0.9	1.000(0.0031)	1.000(0.0045)	0.990(0.0090)
	0.8	0.25	0.923(0.0442)	0.972(0.0659)	0.943(0.0969)
	0.8	hetero	0.932(0.0284)	0.987(0.0444)	0.966(0.0678)
	0.8	0.9	1.000(0.0089)	1.000(0.0182)	0.999(0.0299)

Table S.7: Empirical coverage probabilities at the 95% nominal level (mean absolute errors ↓) under varying quantile levels and truthful response rates, with different values of t_T and a fixed number of $K = 10$ clients. Only 5 out of the 10 clients are randomly selected to participate in each communication round. In Homo, data for each client k are independently drawn from $\mathcal{C}(0, 1)$. In Hete L, client-specific data are independently drawn from $\mathcal{C}(\mu_k, 1)$ with $\mu_k \sim \mathcal{N}(0, 1)$. The label "hetero" indicates heterogeneous truthful response rates with r_k ranging uniformly from 0.25 to 0.9.
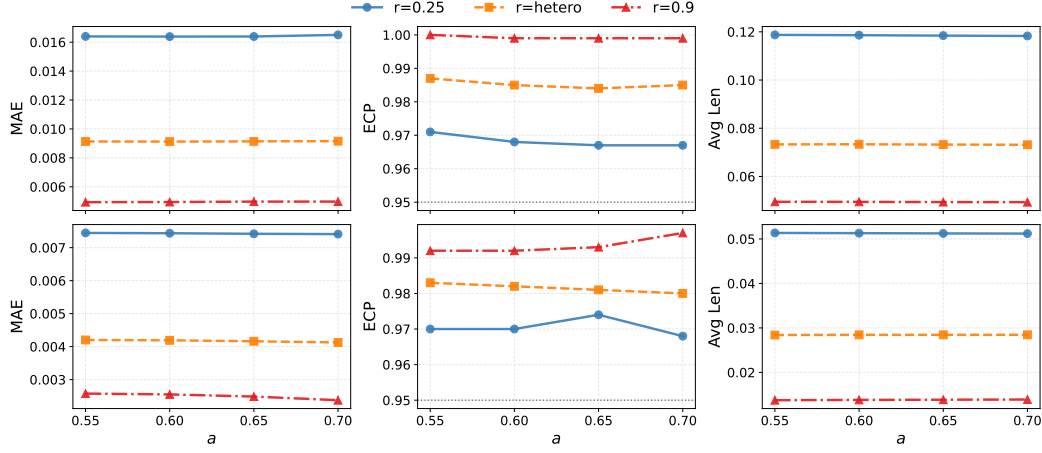
Figure S.4: Mean absolute errors (MAE ↓), empirical coverage probabilities at the 95% nominal level (ECP), and averaged confidence interval lengths (Avg Len ↓) under varying step-size parameter a. We fix $\tau_k \equiv \tau = 0.5$ and $K = 10$, with data generated from $\mathcal{N}(0,1)$. Three response-rate scenarios are considered, where "hetero" indicates heterogeneous client-specific truthful response rates r_k ranging uniformly from 0.25 to 0.9. The upper panels correspond to $t_T = 10,000$, and the lower panels to $t_T = 50,000$.

| Scenario | Quantile (τ) | Rate (r) | Normal | | SN | |
			ECP	Avg Len (10^{-2})	ECP	Avg Len (10^{-2})
	0.5	0.25	0.930	6.215	0.949	8.792
	0.5	hetero	0.946	3.452	0.963	4.566
	0.5	0.9	0.996	1.726	0.995	1.909
	τ_{low}	0.25	0.928	6.411	0.947	9.135
Homo	τ_{low}	hetero	0.947	3.550	0.962	4.709
	τ_{low}	0.9	0.999	1.753	0.999	2.093
	τ_{high}	0.25	0.944	6.681	0.939	9.535
	τ_{high}	hetero	0.942	3.686	0.968	4.914
	τ_{high}	0.9	0.996	1.791	0.996	2.232
	0.3	0.25	0.930	8.504	0.958	12.090
	0.3	hetero	0.951	4.613	0.949	6.404
	0.3	0.9	0.996	2.053	1.000	3.228
	0.5	0.25	0.972	9.439	0.950	10.891
Hete L	0.5	hetero	0.987	5.099	0.952	5.604
	0.5	0.9	1.000	2.200	0.996	2.429
	0.8	0.25	0.997	19.021	0.966	17.014
	0.8	hetero	1.000	10.029	0.962	8.792
	0.8	0.9	0.999	3.488	0.990	4.759
	0.5	0.25	0.938	6.246	0.949	8.848
Hete D	0.5	hetero	0.958	3.469	0.966	4.788
	0.5	0.9	0.998	1.735	1.000	2.524

Table S.8: Empirical coverage probabilities at the 95% nominal level (ECP) and average confidence-interval lengths (Avg Len ↓) for the self-normalized and oracle normal-based confidence intervals. We fix $K = 10$, $E'_m = 1$, and $t_T = 10,000$. Three heterogeneity scenarios are considered. In Homo, data for each client k are independently generated from $\mathcal{N}(0,1)$. In Hete L, data for each client k are independently generated from $\mathcal{N}(\mu_k, 1)$, where $\mu_k \sim \mathcal{N}(0,1)$. In Hete D, data are generated from $\mathcal{N}(0,1)$, $\mathcal{U}(-1,1)$, and $\mathcal{C}(0,1)$ across different clients. "hetero" indicates client-specific truthful response rates r_k range uniformly from $[0.25, 0.9]$.

Scenario	Quantile (τ)	Rate (r)	Normal		SN	
			ECP	Avg Len (10^{-2})	ECP	Avg Len (10^{-2})
	0.5	0.25	0.940	7.792	0.950	10.398
	0.5	hetero	0.953	4.326	0.953	5.906
	0.5	0.9	0.999	2.164	1.000	3.290
	τ_{low}	0.25	0.921	8.657	0.929	11.436
Homo	τ_{low}	hetero	0.897	4.788	0.923	6.215
	τ_{low}	0.9	0.983	2.360	0.969	3.222
	τ_{high}	0.25	0.946	9.811	0.956	13.120
	τ_{high}	hetero	0.955	5.400	0.956	7.578
	τ_{high}	0.9	0.995	2.614	0.999	4.119
	0.3	0.25	0.923	12.044	0.947	17.008
	0.3	hetero	0.947	6.600	0.957	9.670
	0.3	0.9	0.999	3.105	1.000	5.241
	0.5	0.25	0.975	12.495	0.942	13.759
Hete L	0.5	hetero	0.971	6.835	0.946	8.276
	0.5	0.9	0.952	3.179	0.976	5.085
	0.8	0.25	0.999	38.893	0.935	28.048
	0.8	hetero	1.000	20.716	0.956	17.456
	0.8	0.9	0.998	8.240	0.985	10.558

Table S.9: Empirical coverage probabilities at the 95% (ECP) and average confidence-interval lengths (Avg Len ↓) for the self-normalized and oracle normal-based confidence intervals. We fix $K = 10$, $E'_m = 1$, and $t_T = 10,000$. In Homo, data for each client k are independently generated from $\mathcal{C}(0, 1)$. In Hete L, data for each client k are independently generated from $\mathcal{C}(\mu_k, 1)$, where $\mu_k \sim \mathcal{N}(0, 1)$. "hetero" indicates client-specific truthful response rates r_k range uniformly from $[0.25, 0.9]$.

Scenario	Quantile (τ)	Rate (r)	C1	C5	Log
			$t_T = 10000$		
	0.3	hetero	0.937(0.0178)	0.969(0.0271)	0.970(0.0352)
Hete L	0.5	hetero	0.920(0.0142)	0.964(0.0206)	0.974(0.0260)
	0.8	hetero	0.943(0.0261)	0.975(0.0395)	0.975(0.0515)
	0.5	0.25	0.941(0.0141)	0.977(0.0246)	0.988(0.0362)
Hete D	0.5	hetero	0.956(0.0073)	0.981(0.0124)	0.992(0.0172)
	0.5	0.90	0.942(0.0039)	0.994(0.0067)	0.999(0.0097)
			$t_T = 50000$		
	0.3	hetero	0.918(0.0093)	0.950(0.0131)	0.962(0.0178)
Hete L	0.5	hetero	0.901(0.0073)	0.959(0.0101)	0.972(0.0136)
	0.8	hetero	0.908(0.0142)	0.968(0.0191)	0.978(0.0270)
	0.5	0.25	0.941(0.0061)	0.977(0.0082)	0.997(0.0127)
Hete D	0.5	hetero	0.940(0.0034)	0.977(0.0043)	0.997(0.0063)
	0.5	0.90	0.958(0.0016)	0.978(0.0023)	0.998(0.0035)

Table S.10: Empirical coverage probabilities at the 95% nominal level (mean absolute errors ↓) under varying quantile levels and truthful response rates, evaluated under a decentralized ring topology with different values of t_T and a fixed number of $K = 10$ clients. In Hete L, client-specific data are independently drawn from $\mathcal{C}(\mu_k, 1)$ with $\mu_k \sim \mathcal{N}(0, 1)$. In Hete D, data are generated from $\mathcal{N}(0, 1), \mathcal{U}(-1, 1)$, and $\mathcal{C}(0, 1)$ across different clients. The label "hetero" indicates heterogeneous truthful response rates with r_k ranging uniformly from 0.25 to 0.9.